ABSTRACT

POLAT, DAMLA. A Probabilistic Risk Assessment Framework for Wildfire-Induced Releases from Radiologically Contaminated Forests for Risk-Informed Emergency Planning Purposes (Under the direction of Dr. Mihai A. Diaconeasa).

The increasing wildfire trend in the world has also increased the concerns about fires that may occur in many chemically or radiologically contaminated areas. Based on this idea, this thesis presents a framework that demonstrates the necessity of risk-informed emergency planning in radioactively contaminated areas. Based on the large-scale fires in Chernobyl and their effects on the environment, an analysis was made that takes a postulated wildfire as an example that may occur in the contaminated area around the Fukushima Daiichi Nuclear Power Plant. In this analysis, the doses received from inhalation, cloud-shine and ground-shine exposures were calculated with the data obtained from atmospheric dispersion modeling and compared with examples from daily life. In addition, due to the lack of probabilistic risk assessments in the literature evaluating this type of wildfire events, the general probabilistic risk assessment framework has been applied to wildfire-induced releases from radiologically contaminated forests. The applicability of this framework in many fields, such as nuclear and aerospace safety, has already been demonstrated. As a result of the analyses made for postulated wildfire scenarios, it was shown that a forest fire in the Fukushima region has the potential to affect a large area and exceeds the annual limit values and background radiation. On the other hand, it was observed that the doses obtained were quite low compared to the doses encountered in daily life and could be completely avoided with risk-informed emergency planning. The contribution of the probabilistic risk assessment study carried out in areas contaminated with any pollutant to the interventions to be made in the event of a wildfire and the necessity of risk-informed emergency planning have been demonstrated.

A Probabilistic Risk Assessment Framework for Wildfire-Induced Releases from Radiologically Contaminated Forests for Risk-Informed Emergency Planning Purposes

by
Damla Polat

A thesis submitted to the Graduate Faculty of
North Carolina State University
in partial fulfillment of the
requirements for the degree of
Master of Science

Nuclear Engineering

Raleigh, North Carolina
2022

APPROVED BY:

Dr. Mihai A. Diaconeasa Committee Chair	Dr. Xu Wu

Dr. Mohamed Bourham

DEDICATION

I dedicate this thesis firstly to my father Ertan Yuksel, who has always been my number one supporter, and then to my mother Yasemin Yuksel with all my gratitude for her sacrifices and unconditional love, and to my husband Burak Polat for his continued and unfailing love and support.

BIOGRAPHY

Damla Polat was born in Artvin, Turkey, and grew up in Ankara. She graduated from Hacettepe University Nuclear Engineering in 2016. After graduation, she worked as a project engineer for a company and took part in various projects. She also worked on investments in solar energy systems. During this period, she applied and was awarded with a full scholarship by The Republic of Turkey to continue graduate studies in abroad. She came to the USA in 2020 to pursue Master of Science education. After completion, she will continue to work as a nuclear engineer at the Ministry of Energy, The Electricity Generation Corporation (EUAS) in Turkey. She has been married to Burak Polat since 2017.

ACKNOWLEDGMENTS

I would like to express my sincere gratitude to Dr. Mihai A. Diaconeasa for his invaluable assistance, support, and patience in every stage of my research. My gratitude extends to The Republic of Turkey for their great support and sponsorship in pursuing this master’s education. I specially thank to my colleagues in Probabilistic Risk Assessment Group for all their help, guidance, and feedback in my research process. I am grateful to my parents Yasemin and Ertan Yuksel, for raising me in such a brave, enterprising, and successful way and for their motivation 'Raising a girl is raising the world'. I wouldn't be the person who I am today without them. I would also like to thank my husband Burak Polat for never ending support.

TABLE OF CONTENTS

LIST OF TABLES

LIST OF FIGURES

1. INTRODUCTION

Nuclear energy is the largest low-carbon energy source in the world, but the public acceptance is still a divisive issue in many countries. According to the International Atomic Energy Agency (IAEA)'s annual report of 2020, there are 442 units of reactors operating and 52 units of reactors under construction.[1] Although steps are being taken for a net-zero approach and there is a general understanding that nuclear energy can resolve a lot of climate concerns; there is a hesitance to commit to nuclear energy because of the outcomes from atomic weapons and the potential for catastrophic nuclear power plant accidents. In this regard, the fact that people may not adequately be informed also plays an important role. The public, who do not know what they are facing, may have difficulty in embracing nuclear energy. The historical nuclear power plant accidents have an even lower probability of occurrence now. Modern day nuclear power plants are built according to the highest safety standards of any industry and are designed with high safety at a level that can withstand the most severe accident conditions with very low consequences to the people and the environment. In fact, new designs made in the 2010s are designed to secure themselves with completely passive systems, nearly eliminating human error and the need for emergency power. The new safety designs were informed by probabilistic risk assessments. Probabilistic risk assessment (PRA) studies in the nuclear field provide a wide range of analysis opportunities, from which systems fail, their probability of failure is quantified, and the consequences of these failures evaluated.[2] Probabilistic risk assessments of rare and catastrophic events are of particular importance in evaluating postulated initiating events and their effects on the reactor systems. It is necessary to evaluate all available information by taking all uncertainties into account and to quantify risk metrics in terms of frequencies and consequences. Due to the potential for catastrophic effects on the public, the U.S. Nuclear Regulatory Commission (NRC) first published work on implementing probabilistic risk assessment in nuclear reactors with WASH 1400 in 1975.[3] Later, this study was further developed with industry support, and a more detailed risk analysis study was conducted in Nuclear Regulatory Report NUREG-1150, based on five representative nuclear power plants, and probabilistic risk assessment considerations were included in nuclear regulations.[4] In addition, the NRC has also published emergency preparedness and planning regulations that must be followed in the licensing process for nuclear power plants. The procedures published by the NRC prescriptively describe the order of necessary actions during a radiological event and assist plant operators and institutions with decision-making during a radiological situation.[5] Since there is not a specific regulation for wildfires in contaminated areas, the NRC procedures are the first actions applied in cooperation with fire departments.

This thesis conducts a risk study by addressing the contaminated areas around the nuclear power plant accidents, a main reason for the public's fear of nuclear energy. The Chernobyl nuclear power plant accident was the first radiological accident classified as level 7 according to the International Nuclear and Radiological Event Scale (INES) scale and it is still possible to measure the contamination it caused. The consequences were worse than they should have been due to the poor safety culture during the accident and the absence of good risk-informed emergency planning at the time of the accident. Radionuclides stored in the fields around the power plant since the accident in 1986 are still mixed into the atmosphere in various ways. Due to the high fire trend in the climate of Chernobyl and the agricultural activities around it, the wildfires since the accident are one of the biggest reasons for the resuspension. Further, the local radiation monitoring centers have determined that the amount of radiation in the air has increased up to several times, depending on the intensity of the fires. Although there has not been an emergency that threatens public health due to radiation, this situation has caused concern among the people living in the surrounding area and triggered an opposition to nuclear energy.[6]

According to the information available at the time this thesis was written, the last wildfire occurred in 2020 and the radiation threat news that followed formed the motivation of this thesis. Another nuclear power plant accident that was studied in this thesis is the Fukushima Daiichi meltdown that occurred in 2011 and classified as a level 7 on the INES scale. The nuclear power plant sits in a heavily forested area so the in the event of a forest fire, the emergency response teams need to know the expected radiation doses that can and will emerge. This thesis conducts a study on the necessity and general framework of an emergency plan informed by probabilistic risk assessment. The framework and emergency plan focuses on human health and suggests a standard operating procedure in the event of a fire near the accident site. Information was collected on the amount of radionuclides deposited in the environment after the accident with a wide literature review. From the literature review a determination on the amount of radiation the surrounding people would receive with internal and external exposure was done with an atmospheric dispersion modeling according to postulated fire scenarios. The material is prepared for proper identification using risk-informed knowledge in emergency actions. Finally, using the material collected and the risk-informed emergency actions, a general framework of the health effects on the local population in the case of a fire in a radiologically contaminated area was demonstrated.

2. NUCLEAR ACCIDENTS AND ENVIRONMENTAL CONSEQUENCES

The International Nuclear and Radiological Event Scale (INES) is a radiological accident identification tool utilized by the International Atomic Energy Agency (IAEA) and created 1990. The purpose of INES is to categorize all events, with or without release, occurring in facilities and activities containing any radiation source. The INES discusses the consequences that effect the health of workers or the public, as well as the consequences when systems do not work as designed. The classification scale is characterized as 1 to 7. The levels within the scale are defined as shown in Figure 2-1.

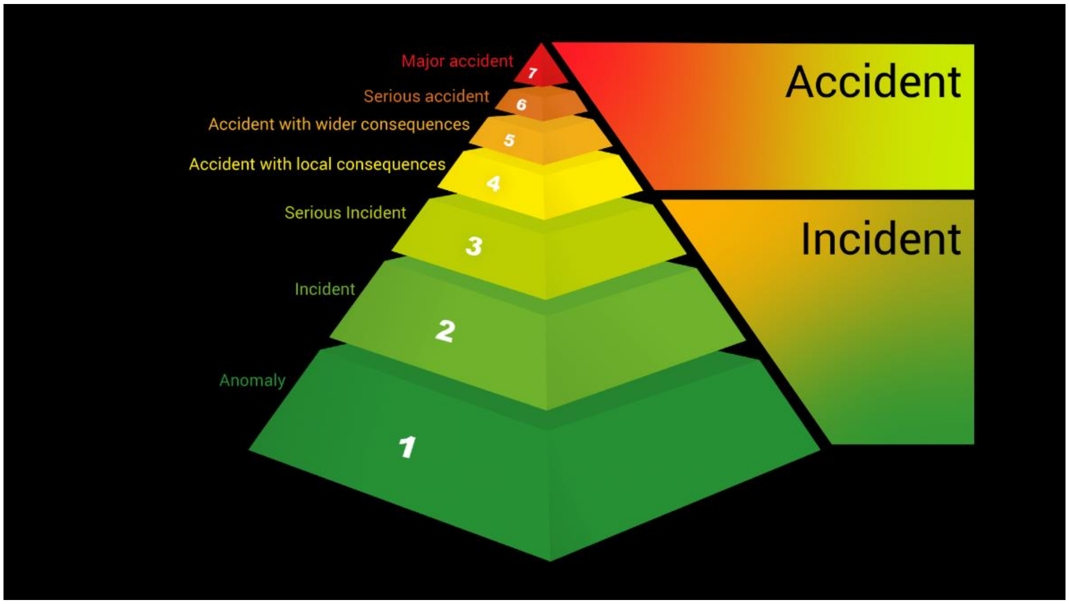

Figure 2-1. INES event scale [7]

To date, there have been two accidents that were classified as a level 7, Chernobyl NPP and Fukushima Daichi accidents. [8] In this section, the timeline and consequences of these two accidents classified as level 7 are briefly explained.

2.1. Chernobyl Nuclear Power Plant Accident

The Chernobyl accident in 1986 was recorded as the largest nuclear accident in history at that time. The failure of the low-power operation test that the Soviet Union wanted to carry out on April 26 resulted in an explosion in the fourth unit and a fire lasting 10 days. As a result, a huge amount of radioactive material was released into the environment and hundreds of thousands of people and habitats around the plant were effected. According to the consequences report published by the IAEA 10 years after the accident, 116,000 people living in the area were evacuated within 4 months after the accident and an 'exclusion zone' with a diameter of 20 km was created around the facility[9]. It stated that less than 10% of the evacuated people were exposed to a dose of 50 mSv, while less than 5% were exposed to a dose of 100 mSv. In addition, 600,000-800,000 people took part in the cleaning and evacuation work called 'liquidation'. Within the first year after the accident, 200,000 workers were exposed to the highest-level dosage of radiation. On average the workers from that first year received an average of 100 mSv doses, while around 10% were exposed to 250 mSv doses, with a strong likelihood that the first responders received fatal dose. Among the teams involved in the accident, 237 people who were occupationally exposed to radiation were identified, and 134 of them were diagnosed with acute radiation syndrome (ARS). Twenty-eight of the patients who had ARS died within the first 3 months. [9]

The Chernobyl accident not only effected the lives of the people living around the plant but also caused a great deal of environmental damage. The deposition of the released radionuclides in forest and grassland areas was dangerous for the vegetation and animals in the region. From the IAEA report the total radioactivity released in the accident was approximately 12×10^{18} Bq. The amount of iodine (I-131) and cesium (Cs-134 and Cs137), which create the biggest concern in the total inventory, is 1.3-1.8×10^{18} and 0.14×10^{18} Bq, respectively. Although the released radionuclides were mostly deposited in the northern hemisphere, the most effected areas were Belarus, Ukraine, and Russia. Areas where the amount of Cs-137 is 185 kBq/m^2, have been estimated as a total of 30,000 km^2 in the three countries while the total are classified as contaminated is 150,000 km^2.[10] The radioactive contamination in milk and agricultural products grown in the region, immediately after the accident was much higher over the acceptable level by the World Health Organization (WHO). Ten years after the accident the contamination in the agricultural products considerably decreased and are now at acceptable levels. However not all consumable products are under the acceptable amount. Food primarily grown in forests such as berries and mushrooms, along with game animals are estimated to have a very high level of Cs-137, with that level remaining high for at least two decades to come.[9] According to the study by Dreicer et al[11], the average Cs-137 deposition in more than 30,000 km^2 of forest area is approximately 37 kBq/m^2, and it exceeds 1.5 MBq/m^2 in 1000 km^2. Although forests are an important resource for the people in the region, since the ecological half-life of cesium in forests is longer, forests pose a danger for longer years compared to agricultural lands. The increased length is due to leaf tissue mixing radioisotopes into the soil. When leaves fall from the trees they dissolve into the soil and water around, mixing the radionuclides into the nutrient sources that feed the trees. The cycle continues, causing radionuclide presence to remain in wilderness longer than agriculture systems.

Chernobyl is a region with a high fire trend caused by straw fires from agricultural activities as well as the climate in the region. A study on wildfires around Chernobyl by Evangeliou et al. in 2015 reveals that the fires of 2002, 2008 and 2010 deposited a cumulative 8% of Cs137 after the accident in 1986 redistributed and caused air contamination in the area[12]. Figure 2-2 displays the radioactive contamination around Chernobyl after the accident. The continuation of wildfires in this region causes radionuclides to continue to affect the surrounding life by resuspending. Although this effect is decreasing over the years, planning and preparedness in such emergencies remain as important factors.

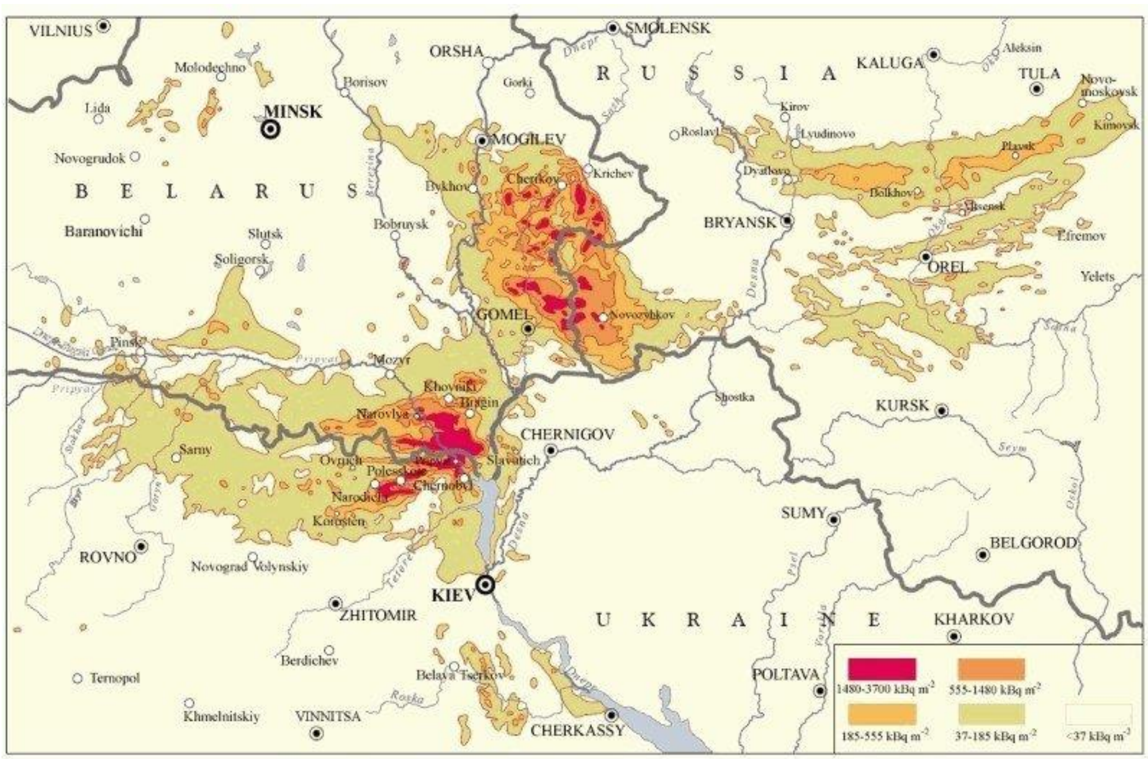

Figure 2-2. UNSCEAR 2000 report, map of radionuclide deposition[13]

2.2. The Fukushima Daiichi Nuclear Power Plant Accident

The Fukushima Daiichi nuclear power plant accident occurred on March 11, 2011, and subsequently transpired as the biggest nuclear accident since Chernobyl. The tsunami that was triggered by an earthquake which had a magnitude of 9 on the Richter scale and lasted more than 2 minutes, flooded the primary and backup power systems and equipment of all 6 units, along with the ultimate heat sink systems. At the time of the earthquake, only 3 units were in operation and were automatically shut down when the earthquake was detected by sensors with control rods inserted as per the safety systems, stopping the nuclear reaction. The plant lost on-site power from the tsunami and a loss of off-site power (LOOP) due to the earthquake. The Fukushima Daiichi Nuclear Power Plant experienced station blackout (SBO) status in Units 1 through 5, lasting nine days in Units 1 and 2, and 14 days in Units 3 and 4. Failure to restore heat removal resulted in fuel meltdown in Units 1, 2, and 3, and radiological leakage began to occur from the damaged reactor pressure vessel (RPV) to the primary containment vessel (PCV). The timeline in Figure 2-3 details the hydrogen formation and subsequent explosions occurred in Units 1, 3, and 4. After the explosion, radioactive substances that had leaked into the containment were released into the environment in a controlled (venting) and uncontrolled (explosions) manner. After the explosions in the three units and the high radiation measurements outside the power plant the Government of Japan issued a 20 km evacuation order along with a mandate for the public to shelter indoors who lives between 20 and 30 km from the plant. [14,15] In the report published by IRSN[16], it was stated that the core in Reactor 1 melted completely, and the entire corium dropped to the base of the containment and ate away a minimum depth of 70 cm. In addition, there was severe damage in Reactor 2 and 3, but a small amount of the core mass dropped to the base of the containment and ate away up to 20 cm from the base. After maintaining the reactor cooling control, the continuation of the cooling of spent fuel pools and the desalination of water began in August 2011. In addition, as of March 2012, when this report was published, the cover built around Reactor 1 was completed and construction scheduled for covering Reactor 3 and 4. The accident had significant environmental consequences. In addition to the dispersion in the form of radioactive gas and fine radioactive particles into the atmosphere, there has been dispersion in the marine environment due to direct release of contaminated water and aerosols resulting from fallout. Shortly after the accident, it was observed that the radiation values of the monitor stations in Tokyo-Shinjuku (250 km from the plant), Tsukuba (170 km from the plant), and Takasaki (250 km from the plant) increased.[17] 78,000 people were evacuated from the area within the 20 km radius, shortly after that 62,000 people from the area between 20-30 km, and then 10,000 more people were evacuated due to the concentration of the radionuclides released from the accident in the northwest direction. When these numbers are considered, more evacuations were made in Fukushima region than Chernobyl which caused evacuation of 116,000 people. While the dose received by those evacuated due to the Chernobyl accident reached 100 mSv, the maximum dose received by the people evacuated from Fukushima was estimated to be 10 mSv. In addition, it was determined that workers involved in post-accident activities received an average dose of 12 mSv, with 1% were exposed to a dose of more than 100 mSv, while six of them were exposed to a dose of 678 mSv. The estimated amount radionuclides released in the accident were 90-700 PBq I-131, 7-20 PBq Cs-137 and 6,000-12,000 PBq Xe-133. [18]

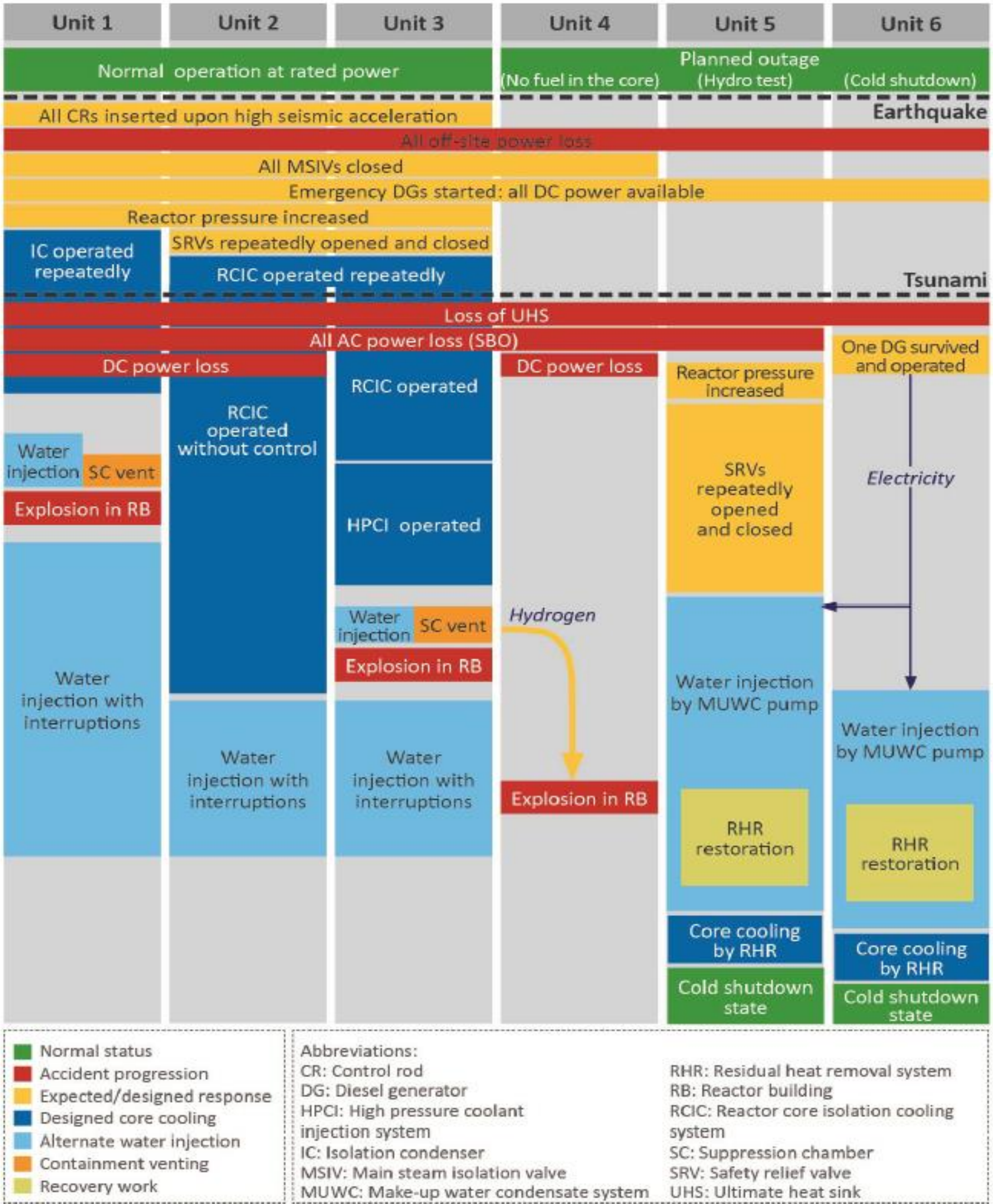

Figure 2-3. Fukushima Daichi NPP accident event sequence [19]

While there was no radiation-related injury or death as a result of the accident, the average effective dose in the following year for the people living in Fukushima city, which is approximately 60 km away, was estimated to be 4 mSv and twice as high for 1 year-old infants.[15]

3. RISK FRAMEWORK FOR WILDFIRE-INDUCED RELEASES FROM RADIOLOGICALLY CONTAMINATED FORESTS

This study uses the 'triplet definition of risk' to review the probability of consequences. [2] The 'triplet definition of risk' is an all-inclusive approach because it incorporates all parameters of risk. The definition consists of three questions that lead to the probabilistic assessment of risk.

1) What can go wrong?

2) How likely is that to happen?

3) What are the consequences if it does happen?

The first question represents possible scenarios for the investigated situation. All possible scenarios that may happen in this step are collected and the end state of these scenarios give the consequences, namely the answer to the third question.[20] The remainder of the work consists of finding the probability of each scenario in the form of numerical data, typically found in historical records or by modeling. According to the questions asked, the definition can be formulized simply as follows,

$$R = \{\langle S_i, L_i, X_i \rangle\}_c \tag{3.1}$$

where R denotes the risk, S_i is the i^{th} risk scenario, L_i is the likelihood of that scenario, X_i is the consequences and the subscript c denotes 'complete' meaning that all the scenarios must be included in the set. Below are steps that need to be followed to carry out a complete probabilistic risk assessment:

Step 1: Defining the normal conditions of the analyzed system to establish the reference point.

Step 2: Identification and characterization of hazards.

Step 3: Developing 'what could go wrong' scenarios.

Step 4: Quantify the probability of each scenario.

Step 5: Assembling the scenarios according to their damage levels and positioning them on the appropriate risk curves and risk priorities.

Step 6: Interpreting results to guide the risk management process.[20]

In the case of a wildfire, studying the events and the following failures to lead to a wildfire can prove difficulty due to dependence on specific regional information. However, events and failures can be grouped into general scenarios, such as climate-related causes, heat waves, deliberate straw burnings, arson, short-circuit fires, fires caused by human error, and home accidents. The European Forest Fire Information System (EFFIS), initiated by the European Commission, is a service that focuses on 43 countries in total, including European countries and a few neighboring Mediterranean countries. According to the annual report published by EEFIS in 2020, more than 66,000 forest fires occurred in 30 countries where data was collected. Among these countries, the biggest burning area belonged to Ukraine. In 2020, 750 km^2 forest area was burned in 2,598 fires in total in Ukraine.[21] In Japan, there was an average of 1,300 wildfires per year between 2015 and 2019.[22] However, in the data obtained before these dates, the average annual number of wildfires was recorded as 4,071 in the 1980s and 3,274 in the 1990s.[23] According to Global Forest Watch Data, 278 of a total of 147,597 forest fires in Japan from 2012 to the present occurred in Fukushima Prefecture.[24] As of June 2022, more than 29,000 fires have been recorded within the US since the beginning of the year, and over 10,000 km^2 have been burned. In 2021, a total area of over 70,000 km^2 was burned with a total number of fires of 58,985.[25,26] In 2020 many intense fires were experienced not only within the US but also in the Chernobyl Exclusion Zone. When we look at the data for the US, more than 100,000 km^2 were burned in a total of 58,950 fires in 2020. 9,917 of this occurred in the state of California, with 43,000 km^2 of burned area.[27] Diablo Canyon Nuclear Power Plant is susceptible to being affected by these fires due to its location in California. Although the decision to shut down the plant has been made, it is still operating and contains spent fuel, which still have high activity and sit in densely filled spent fuel pools and dry cask storage. In addition, the plant resides near an active fault line increasing seismic risks. Even if there is no damage to the main buildings of the power plant, it will cause a great threat to the region if spent fuel pools, pool water pumps, or water supply systems are damaged by earthquakes or wildfires. Since Diablo Canyon is subject to the safety regulations that all other power plants are subject to, and also there is a probabilistic risk assessment study that includes the evaluation of internal and external hazards, very limited considerations have been included regarding a wildfire that may occur in the region.[28]

NRC and licensees have gained significant knowledge and experience on probabilistic risk assessment since 1975. Since the 1990s, efforts have been made to implement probabilistic risk assessment into regulations. Probabilistic risk assessment implantation plans made in the 1990s turned into risk-informed and performance-based regulation implementation plans in the 2000s. NUREG-1150 risk assessment study on five sample nuclear power plants provides a detailed framework for failures that may occur in a nuclear power plant and their consequences. It analyzes the results according to the failure modes, calculates the contribution and probability of core damage in each case. In addition, this study includes off-site consequence analysis and public risks. In Part 50 of the 'NRC Regulations Title 10 Code of Federal Regulations' document, where the criteria to be followed in the licensing process of nuclear power plants are determined, the rules to which nuclear power plants are subject are explained and it is mandatory to have an appropriately prepared emergency planning.[29] There are other documents explaining emergency preparedness and emergency response procedures prepared by NRC and IAEA.[30,31] In addition, although not as strict as nuclear regulations, almost every region has its own fire regulations. However, in addition to all the regulations, there is a lack of a special study for the situations that may cause resuspension in radioactively contaminated regions. The small amount of research done reveals a deficiency in the regulations and considering the big fires seen in Chernobyl, it is considered necessary to make a special planning for this situation.

In case of fires that are the subject of the thesis, the authorities order a warning to the emergency response teams and the people living in the surrounding area to take protective measures in addition to making the necessary interventions. For this, an organized work plan must be made in advance with the administrations in the surrounding cities and towns. In such a case, it becomes a difficult decision-making and implementation process that requires the participation of many institutions and teams.

After the emergency is initiated, the scale and radiological evaluation of the event should be made by the radiological evaluators of the authorized institutions, and the level of precautions should be determined. Accordingly, sheltering, shielding, or evacuation decisions and their cost should be determined, risks should be evaluated, and a final decision should be made. Concurrently to the decision-making process, the spread rate of the fire should be determined by data such as weather conditions, and wind speed, and determined by atmospheric dispersion modeling, as we did here, and coordinated measures against both fire initiation, spread, and radioactive plume dispersion should be discussed.

Personal precautions taken by any level of the response teams also have an important place in this planning. The more protected the crews are, the faster and longer they will be able to respond, directly influencing the management and eventual cease in the fire and emergency. If the sheltering period exceeds 24 hours, it is necessary to meet the food and hygiene needs of the people living in the vicinity. In addition, people staying in buildings such as private care homes, hospitals, and schools will have additional needs, and the city officials must assess the condition of these buildings. For these decisions to be made in an emergency, having a completed probabilistic risk assessment study done will ease a portion of the stress. Thus, it will be easier for the decisions taken to be most cost-effective and for the benefit of the public.

3.1. Frequency of Initiation and Propagation of Wildfires

The initiation and spread of fires depend on many reasons. The reasons to be counted for its initiation can be gathered in three general groups as natural, accidental, and endogenous. Its spread is directly related to the meteorological and topographic structure of the region. The reasons for the start of wildfires are shown in the chart in Figure 3-1 prepared according to the report published by the United States Department of Agriculture in 2013. [32] In Figure 3-2, the contribution of these reasons to the burning areas is seen. Although natural causes occupy a large place among the causes of fire initiation, other causes are also numerically significant. However, considering the effects on the amount of burned areas, it is seen that the biggest contributor cause of area burning is natural causes.

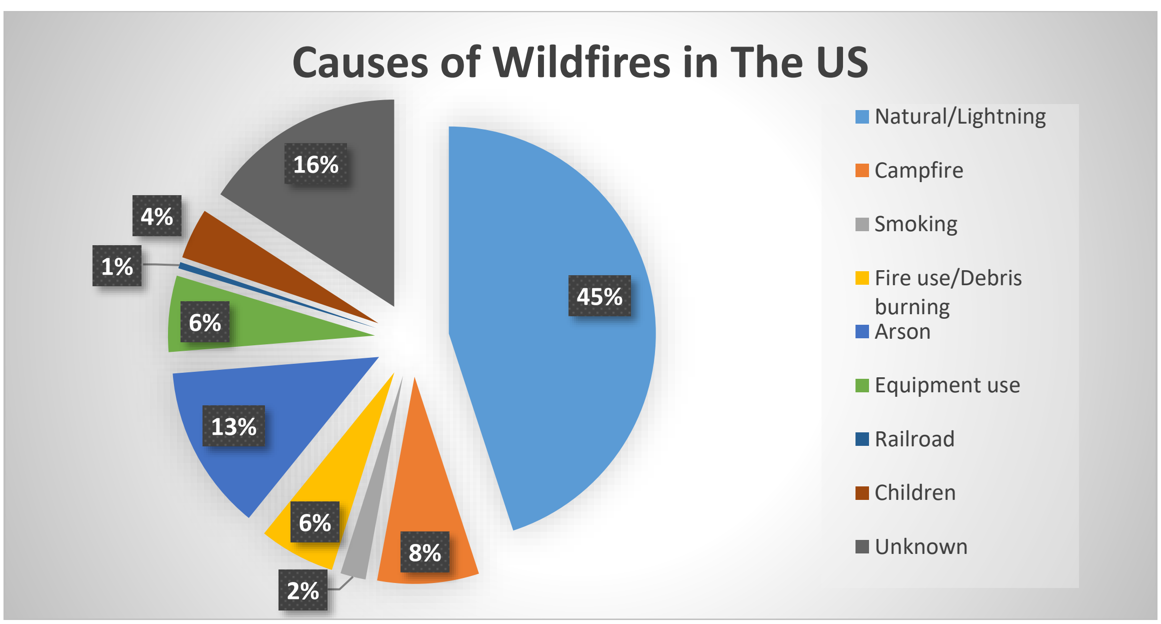

Figure 3-1. Causes of wildland fires in The U.S. (Reproduced from Ref[32]

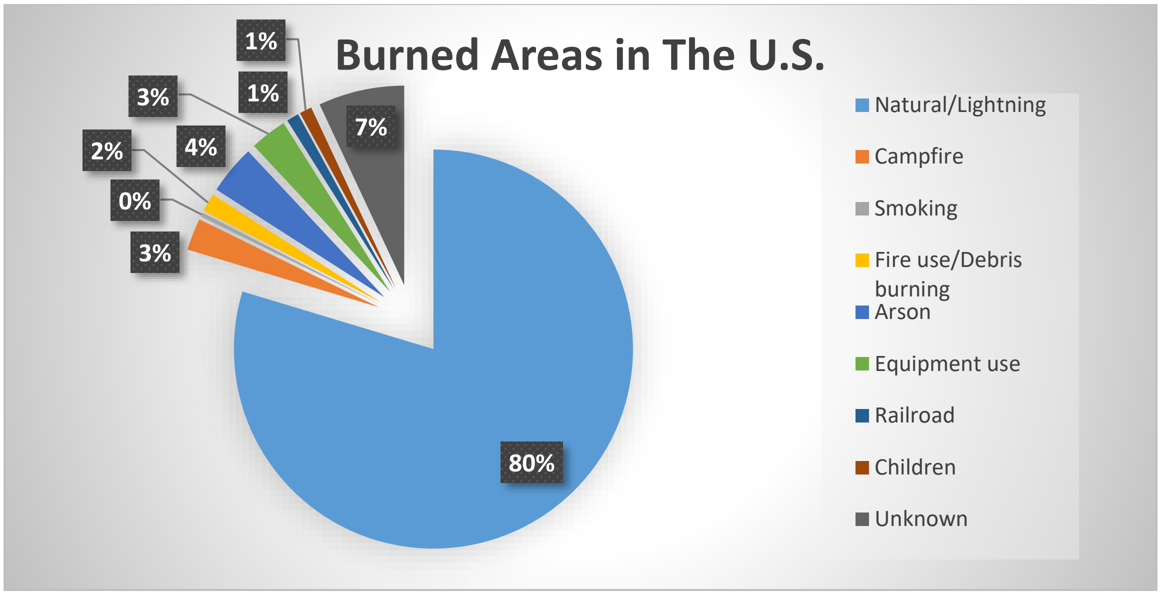

Figure 3-2. Effects of the causes to the burned areas (Reproduced from the Ref[32])

Figure 3-3 shows the causes of wildfires in Japan, based on the information available with limited data, and the effects of each on the total number of fires. Accordingly, the reason for wildfires in Japan is largely human activities. [23] For Ukraine, the situation is similar to that of Japan, apart from the lack of data. While only 2% of the recorded fires in the Chernobyl region initiated with natural causes, the majority of them were attributed to human activities, although 63% of the fires were recorded as unknown causes.

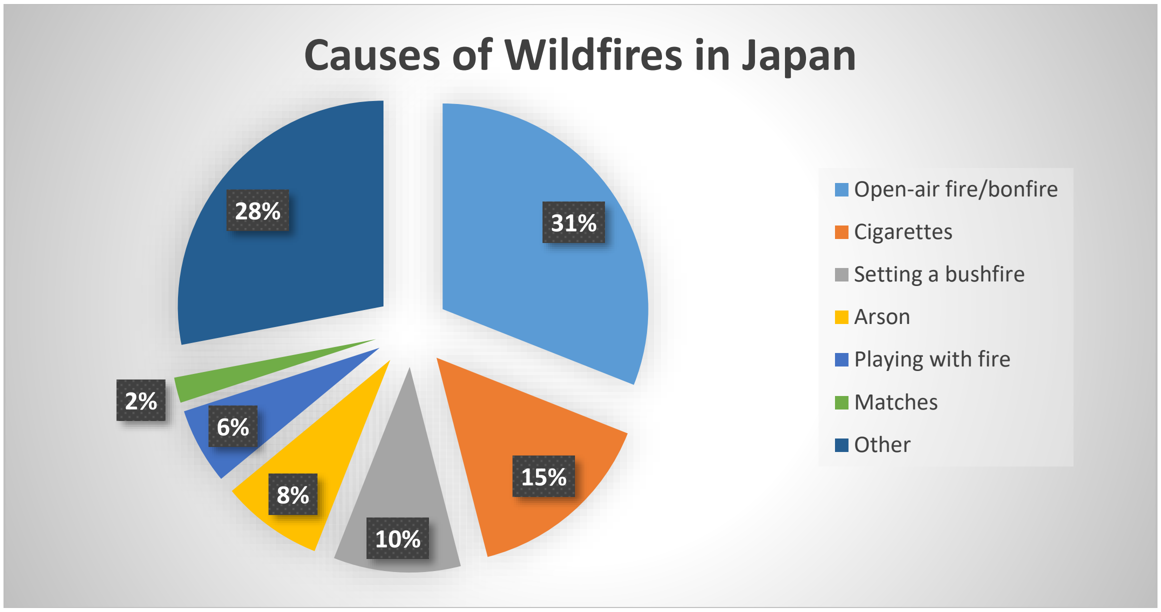

Figure 3-3. Causes of wildland fires in Japan (Reproduced from Ref.[23])

For a complete wildfire risk assessment, fire initiation frequency and fire propagation data should be determined. Frequency data are found by looking at statistical historical records, while fire propagation can be done by means of deterministic simulation modeling to inform the estimation of conditional probabilities of fire spread. For example, considering the fire initiation frequency for the US, 61,255 wildfires per year were recorded in the average of the last 10 years, the minimum number of fires was 47,579 in 2013 and the maximum number of fires was 71,499 in 2017. However, considering the amount of burned area, it is difficult to say that the spread of the fire is directly related to the number of fires. While the average of burned areas for the same period was 7,358,246 acres, the minimum amount was recorded as 3,595,613 acres in 2014 and the maximum amount was recorded as 10,122,336 acres in 2020.[33] In order to have information about fire propagation, simulation modeling should be done using information such as meteorological data, vegetation diversity and density, topography.

3.2. Wildfire-Induced Radiological Releases from Contaminated Forests

Events such as nuclear accidents, tests, or dirty bombings cause radiological contamination in the areas where these events occur, and the radionuclides released into the environment are stored in the soil, vegetation, and underground waters. In such areas, public health is threatened by consumption of local food, drinking of groundwater, industrial or domestic use of vegetation, or fires occurring in the area. It is possible to see the example of fires, which is the focus of this study, often around the Chernobyl accident site. The dangers of such fires that have occurred in the region since the accident have been studied extensively. In one of these studies Kashparov et al. and Yoschenko et al. described the use of controlled fires in a designated forest area with a size 100x200 meters pine forest near the Chernobyl NPP to monitor the amounts of radionuclides resuspended and mixed into the atmosphere [34,35]. They found that during the active burning phase, radioactivity levels increased several hundred times compared to the background radiation level. During the smoldering phase, it increased by tens of times, and the post-fire period, by several times. The Chernobyl area experienced many fires in the past, both as wildfires and straw-burnings by farmers. Throughout the 2015 fire season of the Chernobyl area, two major fires occurred in April and August, raising concerns about second contamination risk around Europe and northern countries. Evangeliou et al. showed that about 10.9 TBq of Cs-137, 1.5 TBq Sr-90, 7.8 GBq of Pu-238, 6.3 GBq of Pu-239, 9.4 GBq of Pu-240, and 29.7 GBq of Am-241 were released by these fires [36]. It was stated in the news at that time that the radioactivity level around Chernobyl NPP was a 16 times higher than normal in the April 2020 fire season.[37–39] Talerko et al. states that cesium values measured in the air increase by 1-4 orders of magnitude, while Protsak et al. states that cesium concentration measurements are observed almost 100 times higher than the background values before fires in their source term estimation article. The total area burned was estimated as 870 km^2 and 630 GBq of Cs-137, 13.5 GBq of Sr-90, and 59 MBq of Pu isotopes released in total. [40–42]

The Fukushima prefecture is 75% covered by forests. Similar to the Chernobyl area, after the Fukushima NPP accident, roughly 50% of the released Cs-137 was deposited on the nearby forest areas[43,44]. Another study conducted by Kato et al. states that the forest area of Fukushima Prefecture contains the 60-70% of the total Cs-137 deposition onto Japanese land.[45] Since the Fukushima region is also a contaminated area like Chernobyl, resuspension of radionuclides is inevitable in such a case, even if the wildfire risk is low.

3.3. Atmospheric Dispersion Modeling

3.3.1. Theoretical Models

Meteorological Data Processing

Atmospheric dispersion models use meteorological data to determine particle or puff location. Since this data cannot be used directly, it is processed by the model with certain processes and made suitable for use. To provide flexibility to the model, each horizontal grid point in meteorological profiles is linearly interpolated to integrate it into the internal terrain-following (σ) coordinate system.

$$\sigma = \frac{Z_{top} - Z_{msl}}{Z_{top} - Z_{gl}} \qquad (3.2)$$

In Equation *(3.2)*, all heights are taken according to mean sea level Z_{msl} and Z_{top} shows the model's top height. All heights of the model above ground level (Z_{gl}) can be selected in any interval. Model supports three different conformal map projections: 1) Stereographic (spherical), 2) Mercator (cylindrical), and 3) Lambert Conformal (conic), and designed to be identical with the meteorological data using a set of universal mapping transformation routines. One of four ways can be used to provide meteorological data fields; pressure-sigma, pressure-absolute, terrain-sigma, hybrid absolute-pressure-sigma. The minimum data required by the model is U, V (horizontal wind components), T (temperature), Z (height), or P (pressure). Moisture and vertical movement data are optional, but rainfall fields are also required if wet deposition is to be calculated.

- **Pressure-Sigma**

Given input data on pressure-sigma surfaces, these surfaces are assumed to be the natural grid of the meteorological model, so humidity is expected as specific humidity and temperature is assumed to be a dry temperature. Therefore, the virtual temperature is first calculated from the specific humidity (Q).

$$T_v = T\,(1 + 0.61Q) \qquad (3.3)$$

Because pressure-sigma data files do not contain heights, heights are calculated for each data level. The hypsometric equation is integrated from the surface to obtain the height of each data level based on the layer mean virtual temperature. Therefore, the height increases between level 1 and 2:

$$\Delta z = R_d\, T_{v12}\, g^{-1} \qquad (3.4)$$

Where R_d is the gas constant 287.04 (J/kg.K), g is the acceleration of gravity, P_1 and P_2 are pressure values at level 1 and 2, and T_{v12} is the average virtual temperature between levels.

If this input data set is available, relative humidity is required in the calculations to determine cloud levels for wet removal, incident solar radiation for dry deposition, and chemical transformations.

- **Pressure-Absolute**

When input data is given on pressure surfaces, the only surface value required is pressure. It is assumed that the heights of the pressure surfaces (Z_P) are relative to msl (mean sea level). Model output areas on absolute pressure surfaces are usually interpolated to these surfaces. The humidity output is expected as relative humidity (RH), while the temperature is assumed to be a virtual temperature (T_v). Surface values are calculated unless otherwise stated. For example, surface temperature (T_0) is generated adiabatically from the lowest data level using input data level-1 temperature (T_1) and pressure (P_1),

$$T_0 = T_1(P_1/P_2)^{-0.286} \qquad (3.5)$$

The height of the ground surface is directly interpolated from the profile.

- **Terrain-Sigma**

As in the previous sections, surface values are computed, if necessary, but the height of the surface is not required as the input data already terrain following. Upper-level data is processed in a similar way to other coordinate systems, except that the terrain-sigma coordinate system of the input data must be converted to the terrain-sigma system of the dispersion model following the same procedure as the internal model data, except using the top scaling height of the meteorological model.

- **Hybrid Absolute-Pressure-Sigma**

A hybrid coordinate system, typical of output fields available from ECMWF (European Center for Medium-Range Weather Forecasting), consists of an absolute pressure added to the pressure-sigma level. The conversion process is almost identical to normal pressure-sigma data as previously described. Input data is defined at the hybrid pressure levels given by,

$$P_k = A_k + B_k P_0 \qquad (3.6)$$

where k represents the level index, P the pressure, P_0 the surface pressure, A a pressure offset and B a sigma value (0-1).

Advection

Atmospheric dispersion models basically rely on these three processes: pollutants move away from the source with a mean wind velocity field, as they move away from the source it expands and disperses on the way and these pollutant plumes can undergo wet and dry deposition. Models are created by the application of these processes and the definition of the pollutant with all its properties. The most common methods used in the field of modeling are Gaussian plume models, Eulerian distribution models, and Lagrangian models. In this work we have used a hybrid system that combines Eulerian grid dispersion and Lagrangian 3-D puff models for a complete trajectory and concentration maps by considering wet and dry deposition, chemical transformations, and radioactive decay.

The advection of a particle or puff is calculated from the average of the three-dimensional velocity vectors for the initial position $P(t)$ and the first-guess position $P'(t + \Delta t)$. Velocity vectors are linearly interpolated in both space and time. The simplest version of this methodology of Lagrangian model is as follows,

First-guess position:

$$P'(t + \Delta t) = P(t) + V(P, t)\, \Delta(t) \qquad (3.7)$$

Final position:

$$P'(t + \Delta t) = P(t) + 0.5\, [V(P, t)\Delta(t)]\, \Delta t \qquad (3.8)$$

The trajectories terminate if the velocity vectors exit the top of the model, but advection continues along the surface if the trajectories coincide with the ground. The integration time step (Δt) may change during simulation. It is calculated from the requirement that the advection distance per time step be less than the grid spacing. The maximum conveying rate U_{max} is determined from the maximum particle/puff conveyance rate during the previous hour. Time steps can vary from 1 minute to 1 hour and are calculated from the relationship,

$$U_{max}(grid - units\ min^{-1})\ \Delta t(min) < 0.75(grid - units) \tag{3.9}$$

The implementation used in this study maps particles or puffs using the horizontal and vertical position calculations described in the sections above for dispersion modelling. In addition, it uses heat and momentum fluxes that the meteorological data provided. If there is no provided data about the fluxes, it calculates the turbulence effect with the wind and temperature profiles and the heat and momentum flux, and the horizontal and vertical mixing coefficients according to the wind speed profile. For detailed information see Ref.[46]

<u>Air Concentration Calculations</u>

When calculating air concentrations, puff distribution can be defined in horizontal and vertical directions or only in horizontal direction. Concentrations for each puff are summed at each time step to all grid points that fall within the puff defined for the top-hat distributions $(\pm 1.54\sigma_i)$, where i indicates z or h, or Gaussian distributions $(\pm 3.0\sigma_h)$. Vertical distributions are always defined as top-line, while horizontal distributions may be either. The incremental concentration contribution by each puff of mass m to a grid point is computed as follows for a top-hat puff,

$$\Delta c = m(\pi r^2 \Delta z)^{-1} \tag{3.10}$$

where vertical extent $\Delta z = 3.08\sigma_z$, and the horizontal radius $r = 1.54\sigma_h$.

And for a Gaussian puff is,

$$\Delta c = m(2\pi\sigma_h^2 \Delta z)^{-1} \exp\left(-0.5x^2/\sigma_h^2\right) \tag{3.11}$$

where x is the distance from the puff center to grid-node.

Particle distributions can be defined in horizontal and vertical directions or only in vertical direction. The particle calculations with a vertical distribution may have either top-hat or Gaussian puff for horizontal distribution. However, particle calculations are summed into a grid-cell rather than computed at a grid-point. A cell is defined at the center of the node and has an area corresponding to the half-way distance to adjacent nodes. The incremental concentration contribution to a cell by a single particle of mass m is defined for a 3D particle,

$$\Delta c = m(\Delta x \Delta y \Delta z)^{-1} \tag{3.12}$$

where $\Delta x, \Delta y, \Delta z$ are the grid cell dimensions. For a particle with a horizontal top-hat distribution, the incremental concentration is the same with the one for the puff distribution as Eq 3.9 but with Δz defined as grid-cell height. Also, if the horizontal distribution is Gaussian, then the incremental concentration is the same as Eq 3.10 with Δz defined as grid-cell height. The incremental concentrations are added to each grid cell or node each advection time step for all particles or puffs that intersect that point. The final average concentration is the incremental sum divided by the number of time steps in the concentration averaging period.

Deposition

There are three ways in the deposition of the pollutant: dry deposition, wet depletion, and radioactive decay. Dry deposition is defined as a deposition velocity or for particles, being equivalent to the gravitational settling or it may be computed using the resistance method and information about the nature of the surface. Wet removal can be defined for soluble gases by specifying its Henry's Law constant. Gaseous wet removal only occurs for the fraction of the pollutant below the cloud top. Particle wet removal is defined by a scavenging ratio (ℓ/ℓ) within the cloud and by an explicit scavenging coefficient (s^{-1}) for pollutants below the cloud base. The simplest method for calculating the total deposition from both wet and dry removal is expressed in terms of reciprocal time constants of β_{dry} for dry deposition, β_{gas} for wet removal of gases, β_{inc} for in-cloud we removal of particles, and β_{bel} for below-cloud wet removal of particles.

$$D_{wet+dry} = m\left\{1 - exp\left[-\Delta t(\beta_{dry} + \beta_{gas} + \beta_{inc} + \beta_{bel})\right]\right\} \tag{3.13}$$

Particle settling for dry deposition is calculated as follows,

$$V_g = d_p^2\, g\, \left(\rho_g - \rho\right)(18\mu)^{-1} \tag{3.14}$$

where V_g is settling velocity, d_p particle diameter, ρ air density, ρ_g particle density, and μ dynamic viscosity of air $0.01789\, g^{-1}s^{-1}$. Settling velocity has correction factors of slip correction for small particles (C_c) and dynamic shape factor for non-spherical particles (α).

If the assumption of uniform vertical concentration has made then the dry deposition may be calculated as follows,

$$D_{dry} = V_d C \tag{3.15}$$

Wet removal is divided into two parts as below-cloud and in-cloud deposition. In-cloud process contains a scavenging ratio, which is the ration of the pollutant's concentration in water to its concentration in air, and defines as the deposition velocity,

$$V_{inc} = S\, P \tag{3.16}$$

where P is the precipitation ratio. And time constant for in-cloud removal is,

$$\beta_{inc} = F^t F_b V_{inc} \Delta Z_p^{-1} \tag{3.17}$$

where the average scavenging ratio is $S = 5x105\ to\ 1x106$, ΔZ_p is the depth of the pollutant layer for puffs and depth of the cloud layer for particles, F^t is the fraction of the pollutant layer below the cloud top, and F_b is the fraction of pollutant layer above cloud bottom.

Below-cloud removal is defined directly as a rate constant in s^{-1},

$$\beta_{bel} = 1 \times 10^{-6}(1.0 - F_b) \tag{3.18}$$

Wet deposition of gases depends on their solubility and gaseous wet deposition velocity is defined as,

$$V_{gas} = H\ R\ T\ P \tag{3.19}$$

where H is the Henry's Law constant, R is the universal gas constant, T is temperature, and P is the pressure. The gaseous wet removal time constant can be calculated,

$$\beta_{gas} = F^t V_{gas} \Delta Z_p^{-1} \tag{3.20}$$

Radioactive decay is not a part of the deposition itself but since the deposited radioactive pollutants do decay, deposition amounts are adjusted for this process in each time step.

$$\beta_{rad} = ln2/T_{1/2} \tag{3.21}$$

$$m_1 = m_2\ \exp\left(-\beta_{rad} \Delta t\right) \tag{3.22}$$

where $T_{1/2}$ is the half-life of the pollutant.

For the use of different pressure models, detailed explanation can be found in the HYSPLIT supplemental document Ref. [46].

3.3.2. HYSPLIT Software

The Hybrid Single-Particle Lagrangian Integrated Trajectory (HYSPLIT) software is an atmospheric dispersion modeling tool for simulating the pollutant behavior by its physical and chemical properties with the meteorological data of the incident location developed by the National Oceanic and Atmospheric Administration (NOAA) Air Resources Laboratory (ARL) in the early 1980s. This code is suitable for any dispersion scenario to create trajectory and air concentration models with puff or particle approaches. It is a comprehensive modeling system capable of simulating trajectory extraction, transport, dispersion, chemical transformation, and deposition. HYSPLIT code uses both Eulerian and Lagrangian methods where which one is advantageous. While the Lagrangian model is advantageous in distributions closer to the source with a single-source emission, the Eulerian model is more advantageous when modeling distributions on a global scale with multiple emission locations and times, and the HYSPLIT program uses the more advantageous model according to the defined scenario. HYSPLIT is capable to process meteorological data and extracting the trajectory of the particle according to the factors such as pressure, speed, direction, and temperature in this data. In addition, it optimizes the emission masses according to the grid resolution in which the meteorological data is defined and determines the concentration in the grids by using the advantages of modeling as puff on the horizontal and as particles on the vertical. HYSPLIT calculates concentration and trajectory modeling, as well as deposition and decay. Dry and wet deposition and radioactive decays are separated from air concentrations during the modeling period according to the defined deposition speed and half-lives. Also, the solubility of the particle or gas is taken into account when separating the depositions. In doing this, the code yields result as precise as the meteorological data. Any error in the data will cause the HYSPLIT to output an incorrect trajectory.[47–49]

As a result, it is appropriate to use the HYSPLIT code for this study due to its advanced calculation methods, ease of accessing the air concentration and ground deposition values separately, its clarity in showing the results, working on the actual map and being able to be shaped according to various scenarios.

3.4. Radiological Dose Consequences

3.4.1. Theoretical Models

In daily life, people encounter radiation in many places other than the radiation originating from space and the surrounding natural resources. As depicted in Figure 3-4, apart from extraordinary causes such as atomic bombs, nuclear power plant accidents, and nuclear fallout, a large part of the radiation received in daily lives originates from medical imaging.

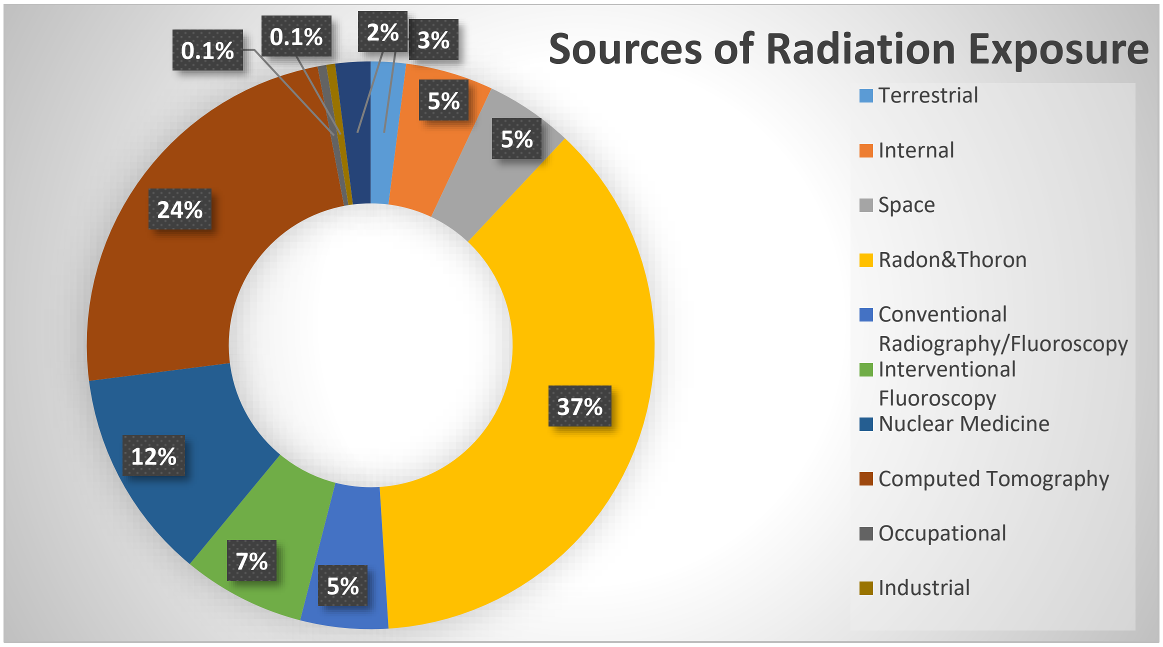

Figure 3-4. Sources of radiation chart (Reproduced from Ref. [50])

For reference, Figure 3-5 shows representative dose examples taken in situations encountered in daily life in Sieverts.

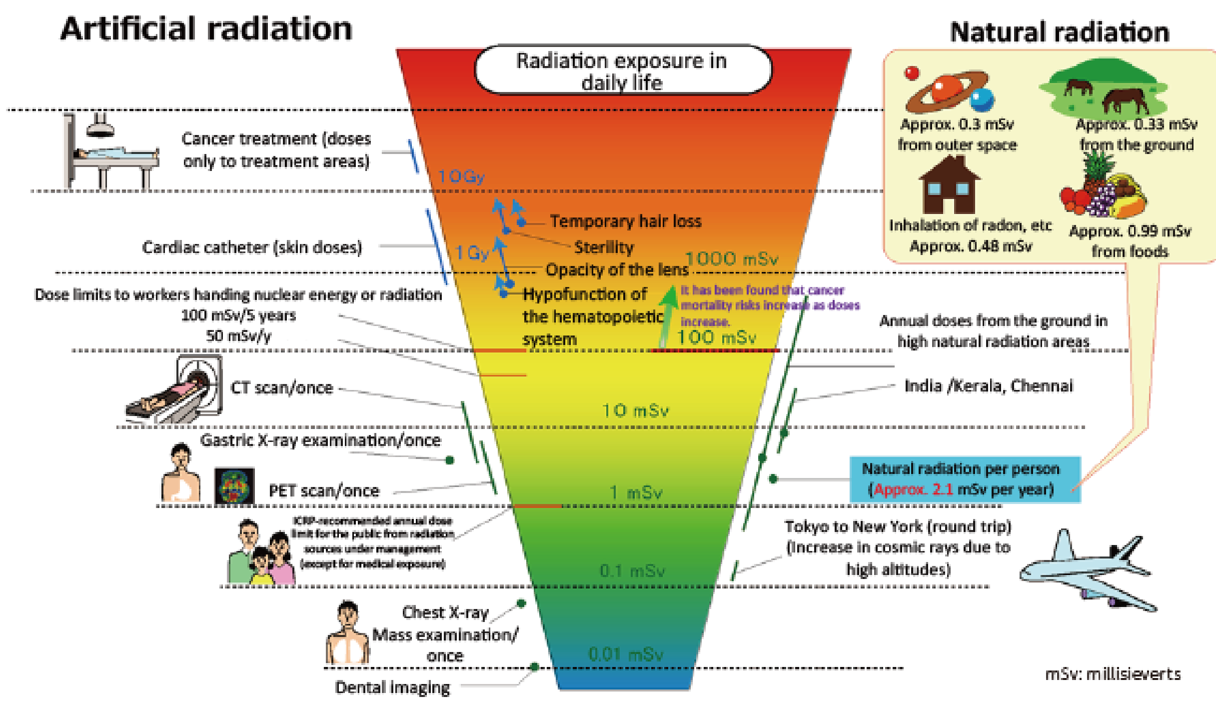

Figure 3-5. Dose chart in Sievert[51]

Medical imaging and applications are the factors that provide the highest contribution compared to other radiation sources. In Table 3-1, the exposure doses are given for the most frequent medical imaging procedures. However, although it has a great place in our lives, a consensus on the effects of chronic low doses of radiation has not been reached yet, and the debate on this topic continues. [52] The most common model used for the effects of low-dose radiation is the linear non threshold hypothesis, however a definite conclusion could not be reached due to the general opinion that this hypothesis is an overestimation of consequences and due to insufficient data on human. On the one hand, there is the idea that radiation is harmful but there must be a threshold, and on the other is the idea of radiation hormesis, which argues that cells respond positively to radiation. [52] In the light of these information, although no clear result can be given regarding the effect of low-dose radiation, it would be a logical approach to compare the low doses with the situations we encounter in our daily lives.

Table 3-1. Medical Procedure Doses in Daily Life Prepared by NRC[53]

Medical Procedure Doses	
Procedures	Doses(mSv)
X-Rays Single Exposure	
Pelvis	0.7
Abdomen	0.6
Chest	0.1
Dental	0.015
Hand/Foot	0.005
Mammogram (2 views)	0.72
Nuclear Medicine	4
CT	
Full body	10
Chest	7
Head	2

Contrary to the effects of low-dose radiation the effects of radiation in large and acute doses have been well understood by all the studies and experiments that have been done. Furthermore, studies are underway on non-repeating acute doses up to 100-200 mSv, acute and repeated doses of several tens of mSv, and long-lasting but low chronic doses. The early effects of acute and large doses are listed in Table 3-2. The early effects are simply those that appear within 60 days of receiving the dose, while the late effects are those that may occur after this time. Early effects are defined acute radiation syndrome at high doses.

Table 3-2. Probable Early Effects of Acute Whole-Body Radiation Doses, Reproduced from Ref.[52]

Acute Dose(mSv)	Probable Observed Effects
50 to 750	Chromosomal aberrations and temporary depression of white blood cell levels in some individuals. No other observable effects.
750 to 2000	Vomiting in 5 to 50% of exposed individuals within a few hours, with fatigue and loss of appetite. Moderate blood changes. Recovery within a few weeks for most symptoms.
2000 to 6000	For doses of 3 Sv or more, all exposed individuals will exhibit vomiting within 2 hours. Severe blood changes, with hemorrhage and increased susceptibility of infection, particularly at the higher doses. Loss of hair after 2 weeks for doses over 3 Sv. Recovery from 1 month to a year for most individuals at the lower end of the dose range, only 20% survive at the upper end of the range.
6000 to 10000	Vomiting within 1 hour. Severe blood changes, hemorrhage, infection, and loss of hair. From 80% to 100% of exposed individuals will succumb within 2 months, those who survive will be convalescent over a long period.

Late effects cause various diseases, especially cancer and cardiovascular diseases, and even if the radiation can penetrate into the cell and cause changes in the chromosomes, this may also cause genetic effects. In radiation-induced diseases, there is a latent period that varies according to age, in which no symptoms are observed, and then a plateau period that during which the cancer risk is constant and defined by the quantitative risk measured by annual cancer incidence rates, after which the risk of developing cancer drops to zero. That is, if there is a cancer that starts to develop in the latent period, it is expected to be seen in the plateau period according to the risk coefficients.

Table 3-3 contains the risk coefficients of radiation induced cancers by type and the age at which the dose is received.

Table 3-3. Radiation-induced Cancer Risk Coefficients Reproduced from Ref.[54]

Type of Cancer	Age at Time of Irradiation	Latent Period (years)	Plateau Period (years)	Risk Coefficient (deaths/10^6/yr/rem)
Bone	0-19.9	10	30	0.4
	20+	10	30	0.2
Breast	10+	15	30	1.5
Leukemia	In utero	0	10	15
	0-9.9	2	25	2
	10+	2	25	1
Lung, respiratory system	10+	15	30	1.3
Pancreas	10+	15	30	0.2
Stomach	10+	15	30	0.6
Rest of alimentary canal	10+	15	30	0.2
Thyroid	0+	10	30	0.43
All other	In utero	0	10	15
	0-9.9	15	30	0.6
	10+	15	30	1

3.4.1.1. Inhalation Exposure Dose

Inhalation exposure is the result of breathing in air contaminated with pollutants. To calculate the radioactive inhalation exposure, it is necessary to know the radionuclide concentration in the contaminated air, how long this air is inhaled, and the inhalation dose coefficient, which varies according to the type of radionuclide. The general model [55] used for this calculation is as follows:

$$Intake = Air\ Concentration\ of\ Radionuclide\ \times Breathing\ Rate \times Exposure\ Time \tag{3.23}$$

$$Inhalation\ Dose = \sum_i Intake_i \times DCC_i \tag{3.24}$$

$$D_{inh}^{i} = C_{air}^{i} \times InhR \times DCC_{inh}^{i} \times t \tag{3.25}$$

where:

D_{inh}^{i} is the inhalation dose from the nuclide i in [Sv/hr]

C_{air}^{i} is air concentration of the nuclide i in [Bq/m^3]

$InhR$ is breathing rate in[m^3/h]

DCC_{inh}^{i} is the dose coefficient for inhalation of the nuclide i in [Sv/Bq]

t is the time of exposure in [hours]

3.4.1.2. Cloud-Shine Exposure Dose

One of the external pathways of radiation exposure is cloud-shine exposure. In this way, the radioactive plume spread after the fire exposes the population in the areas it passes through. The concentration of radionuclide in the air is important in cloud-shine dose calculation. The model used to calculate the cloud-shine exposure dose is as follows,

$$D_{cld}^{i} = C_{air}^{i} \times DCC_{cld}^{i} \times t \tag{3.26}$$

where:

D_{cld}^{i} is the cloud-shine dose from the nuclide i in [Sv/hr]

C_{air}^{i} is air concentration of the nuclide i in [Bq/m^3]

DCC_{cld}^{i} is the dose coefficient for cloud-shine exposure from the nuclide i in [Sv/Bq-hr-m^3]

t is the time of exposure in [hours]

3.4.1.3. Ground-Shine Exposure Dose

Another external exposure pathway is ground-shine exposure. In ground-shine exposure, radionuclides in the ground due to radiological events or mineral sources cause the organisms living on this ground to be exposed to radiation. The ground-shine dose is calculated with the following model,

$$D_{grd}^{i} = CL_{ground}^{i} \times DCC_{grd}^{i} \times t \quad (3.27)$$

where:

D_{grd}^{i} is the ground-shine dose from the nuclide i in [Sv/hr]

CL_{ground}^{i} is contamination level of the nuclide i in [Bq/m^2]

DCC_{grd}^{i} is the dose coefficient for ground-shine of the nuclide i in [Sv/Bq-hr-m^2]

t is the time of exposure in [hours]

3.4.1.4. Ingestion Exposure Dose

Ingestion exposure is one of the biggest contributors to future health risk assessments because the contaminated soil and water continue to contaminate the food or drinking water for years:

$$D_{ingFood}^{i} = IR_{C} \times C_{Diet}^{i} \times DCC_{ing}^{i} \quad (3.29)$$

where:

$D_{ingFood}^{i}$ is the ingestion dose from the nuclide i in [Sv/y]

IR_{C} is the yearly intake of carbon by an individual [kg C/y]

C_{Diet}^{i} is concentration of the nuclide i in the diet [Bq/m^2]

DCC_{ing}^{i} is the dose coefficient for ingestion of the nuclide i in [Sv/Bq]

For water intake:

$$D^i_{ingWater} = IR_W \times C^i_{water} \times DCC^i_{ing} \tag{3.28}$$

where:

$D^i_{ingFood}$ is the ingestion dose from the nuclide i in [Sv/y]

IR_C is the yearly consumption of water by an individual [m^3/y]

C^i_{Diet} is concentration of the nuclide i in drinking water [Bq/m^2]

DCC^i_{ing} is the dose coefficient for ingestion of the nuclide i in [Sv/Bq]

4. PRELIMINARY APPLICATION FOR THE FUKUSHIMA DAIICHI REGION

4.1. Wildfire Frequencies in the Fukushima Daiichi Region

Chernobyl is a region that is likely to experience more climate-related wildfires however, the situation for Fukushima is a little different from Chernobyl. Since the Fukushima region has a humid climate, and the highest average temperature is 25 degrees Celsius even in August, drought and climate-related fires are not likely to happen in the near future. As shown in Figure 3-3 in Section 3.1, possibilities other than this reason such as human-caused, arson, home accidents, etc. always remain as the most likely events that can happen. In addition, the high forest coverage of Fukushima also increases the likelihood that any simple house fire will easily turn into a forest fire. Since 2012 according to the Global Forest Watch data, a total of 32,021 and 278 forest fires were detected in Kyiv, Ukraine, and Fukushima, Japan, respectively. According to a study by Satoh et al in 2004, Japan experiences 3,000 wildfires per year, while the fire intensity is about the same as the United States when comparing the area and number of fires. In this study, it is said that there are 8 fires per 1,000 km^2 per year, and it would be safe to say that this number can be halved according to the most recent data of 1300 wildfires per year and 377,975 km^2 land area of Japan.[56]

4.2. Radiological Releases in the Fukushima Daiichi Region

After the accident, many different institutions and researchers conducted a release evaluation. In these studies, I-131, Cs-134 and Cs-137 were found in drinking water, food, and nature. Japanese authorities took the necessary precautions to prevent contaminated food and drink from being consumed, and the consumption of local products was restricted. In addition, health screenings of the people who lived in the vicinity and were removed from the evacuation zone after the accident were carried out and they were followed up afterward. According to the report published by the IAEA shortly after the accident, the estimated total releases are 90-700 PBq of I-131, 7-20 PBq of Cs-137, and 6,000-12,000 PBq of Xe-133 [57]. Although the Cs-137 deposition was 2-3 PBq, it was estimated that the release amounts were higher in some studies conducted later. Maximum Cs-137 emission was determined as 53.1 PBq in Stohl's study[58], 69.7 PBq in Evangeliou's study[59], and 13 PBq in Katata et al.'s early estimation study[60]. It has been announced that a total area of 30,000 km^2 was effected, in addition to the Japanese authorized ministry declaring the area of 20 km in diameter, approximately 600 km^2 area, around the NPP highly radioactive. Radionuclide concentration was observed hundreds of kilometers away around the nuclear power plant, but the heavily contaminated area with the cesium concentration measured above 1000 kBq/m^2 is mostly 60 km around the power plant.[61]

4.3. Radiological Dispersion Model Assumptions and Parameters

In this section, the scenario and the analysis and results are explained. Because its higher mobility in biomass and longer half-life, Cs-137 was focused on deposition, distribution, and exposure calculations. To run HYSPLIT, a postulated wildfire scenario was created. While creating the scenario, the assumptions about intensity and duration of the fire were decided. According to the literature review conducted, a wildfire is the most intense fire and assumed that 100% of the radionuclides deposited in the forest area would undergo resuspension. In addition, there is no clear information about deposition values in the literature, and values between 2 PBq and 13 PBq of Cs-137 are estimated. Therefore, to present a sensitivity study, values between 5-15 PBq were assumed. This approach allows for the consideration in resuspension of radionuclides deposited in the vegetation as well as the resuspension of the radionuclides deposited to a depth of 5-10 cm in the soil. Thus, a more comprehensive assumption that considers most of the Cs-137 will be released during a fire is made. As seen in the deposition density map in Figure 4-1 the contaminated area with Cs-137 is roughly 50% of the Fukushima Prefecture and 75% of the region is forested. Since the surrounding of the facility is a mountainous and forested, it is a safe assumption that the general structure of Fukushima Prefecture is valid in this area and the same percentages are calculated.

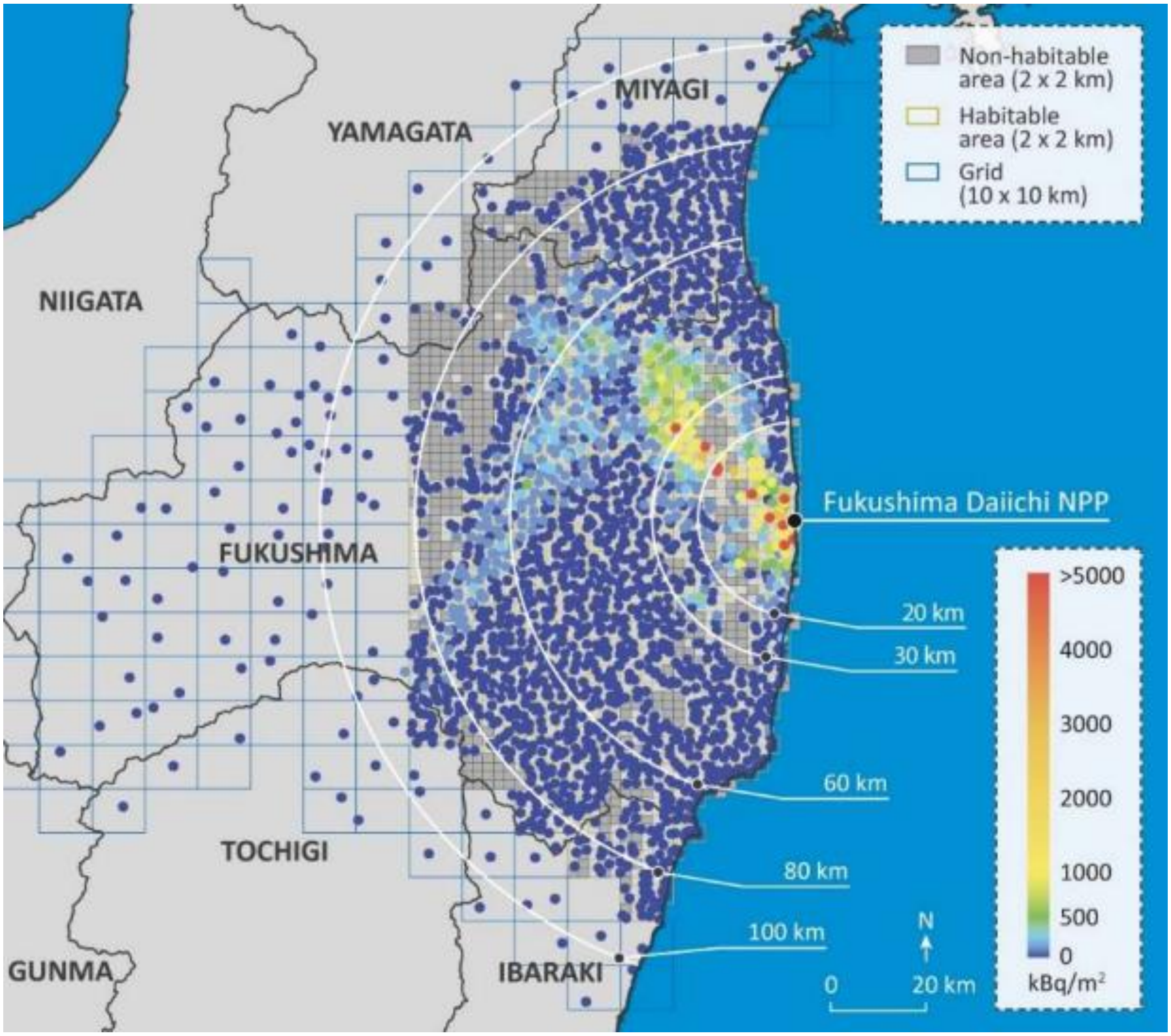

Figure 4-1. Deposition density map of Cs-137[44]

According to the scenario, 20% of this forest area is on fire. In this case, the amount of radionuclides undergoing resuspension are calculated by multiplying the deposition values we used by the factors of 0.75 and 0.20. To determine the fire area, the total area of Fukushima prefecture is multiplied by 0.75 and 0.20, and 0.50 to narrow the area to the contaminated part. According to Figure 4-1, Cs-137 was deposited roughly in half of the Fukushima prefecture. Knowing the total area is 13,784 km^2, after applying the factors, the wildfire area was approximately 1000 km^2. The amount of emission per hour was entered as the program input in the fire that we designed to last for 24 hours. That is, the found emission per hour values by dividing the deposition amounts that were multiplied by the factors 0.75, 0.20, and 0.5 by 24 as seen in Table 4-1.

Table 4-1. Emission Rates

Total Deposition (Bq)	Total Emission (Bq)	Per Hour Emission (Bq/hr)
5.00E+15	7.50E+14	3.13E+13
6.00E+15	9.00E+14	3.75E+13
7.00E+15	1.05E+15	4.38E+13
8.00E+15	1.20E+15	5.00E+13
9.00E+15	1.35E+15	5.63E+13
1.00E+16	1.50E+15	6.25E+13
1.10E+16	1.65E+15	6.88E+13
1.20E+16	1.80E+15	7.50E+13
1.30E+16	1.95E+15	8.13E+13
1.40E+16	2.10E+15	8.75E+13
1.50E+16	2.25E+15	9.38E+13

The distribution of radionuclides after the fire and the change of the dose concentration was followed in the air after the fire by running the HYSPLIT code for a total of 48 hours, the first 24 hours of which the wildfire is burning. Thus, in such a scenario, the opportunity to make a preliminary estimation for the processes of the Cs-137 concentration in the air to go above and below the limits was performed and the corresponding emergency measures to be taken were explored.

4.4. Radiological Dose Results

Natural and artificial radionuclides constitute the source of radiation in atmospheric, terrestrial, and aquatic environments, and radioactivity concentrations in these environments are rapidly increasing locally and regionally as a result of human activities.

Radionuclides, which are naturally present in our environment or released into the environment as a result of human activities, are in continuous motion in the air, water, and soil. Radionuclides can move from one region to another by winds and can be deposited in the soil and water by dry fallout or precipitation. It can be transported to lakes and seas by rivers, mixes with the soil again with irrigation, mixes with underground waters, and can cause bioaccumulation by transferring from water and soil to living things.

Radionuclides blended into the environment due to radiological accidents resuspends by disasters such as wildfire, mix with nature again in the same ways, and affect public health. The radiation that exists naturally around us without any radiological accident or effect is called background radiation, and although it varies between 1-10 mSv/year on the world, the average effective background dose is 2.4 mSv/year. According to the radiation exposure limits determined by the IAEA and generally accepted by the nuclear authorities of other countries, the annual dose limit for individual members of the public is 1 mSv, excluding background radiation. [62]

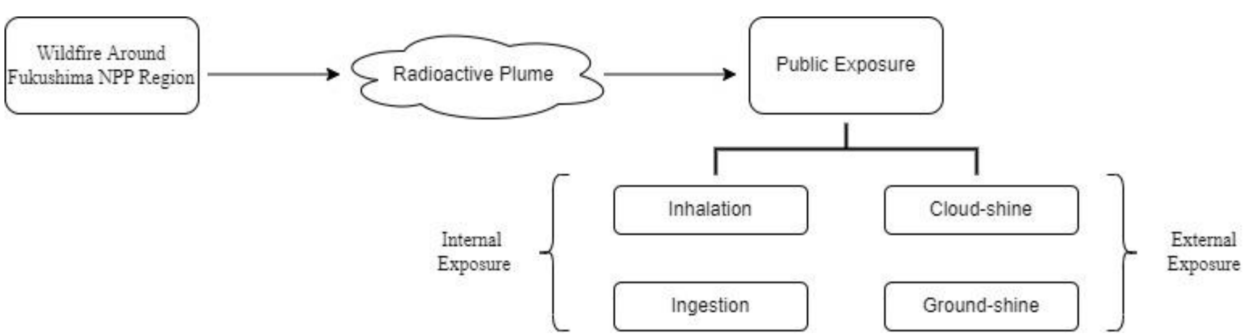

Figure 4-2. Radionuclide transport due to wildfires

In this study, the calculation of external and internal exposure that the people living in the surrounding area will be exposed to due to a wildfire event that may occur around the Fukushima nuclear power plant has been calculated. Figure 4-2 demonstrates a simple diagram of the scenario created. While calculating the received doses, calculations were made in three different categories as inhalation, cloud-shine, and ground-shine radiation. While determining these three categories, the ways of exposure that will affect the population living around the fire were taken into account, and the results and effects of each calculation will be explained in detail in the following sections. Since the scenario considered is similar to the early (first few hours) and mid-phase (first days or weeks) processes of a nuclear accident, the most important exposure routes are inhalation, ground-shine, and cloud-shine.[31] Apart from these three ways, we did not include ingestion, which has a great long-term effect, in our calculations because we examined the short-term effects. For a comprehensive study, the dietary habits of the population, the amount of consumption and the examination of the paths followed by radionuclides in nature are required. When calculating all these exposures, we assume that people spend half of the day indoors and the other half outside without any shielding. The general house structure around the Fukushima NPP is 1-2 story wooden framed. Considering this building structure and the calculations made by the Japanese government after the accident for analyzes, we used a reduction factor for indoor times. According to Table 4-2, this factor is determined as 0.4 for 1-2 story wooden frame houses.

Table 4-2. Reduction factors for surface deposition (Reproduced from Ref. [30])

Structure or Location	Representative Shielding Factors	Representative Range
1 m above an infinite smooth surface	1	-
1 m above ordinary ground	0.7	0.47-0.85
One- and two-story wood-frame house (no basement)	0.4	0.2-0.5
One- and two-story block and brick house (no basement)	0.2	0.04-0.4
House basement, one or two walls fully exposed - One-story, less than 1 m of basement wall exposed - Two-story, less than 1m of basement wall exposed	 0.1 0.05	 0.03-0.15 0.03-0.07
Three or Four story structures (500 to 1000 m^2 per floor) - First and second floor - Basement	 0.05 0.01	 0.01-0.08 0.001-0.07
Multi-story structures (>1000 m^2 per floor) - Upper floors - Basement	 0.01 0.005	 0.001-0.02 0.001-0.15

In addition, these calculated doses were compared with the background radiation and radiation limit, and these comparisons were visualized with graphics in each section of exposures.

The distribution maps shown in the Figure 4-3 to 15 were obtained according to the results of the atmospheric distribution study performed by applying the given assumptions. Thus, the direction and distance to which resuspending radionuclides will be transported in case of wildfire were visualized.

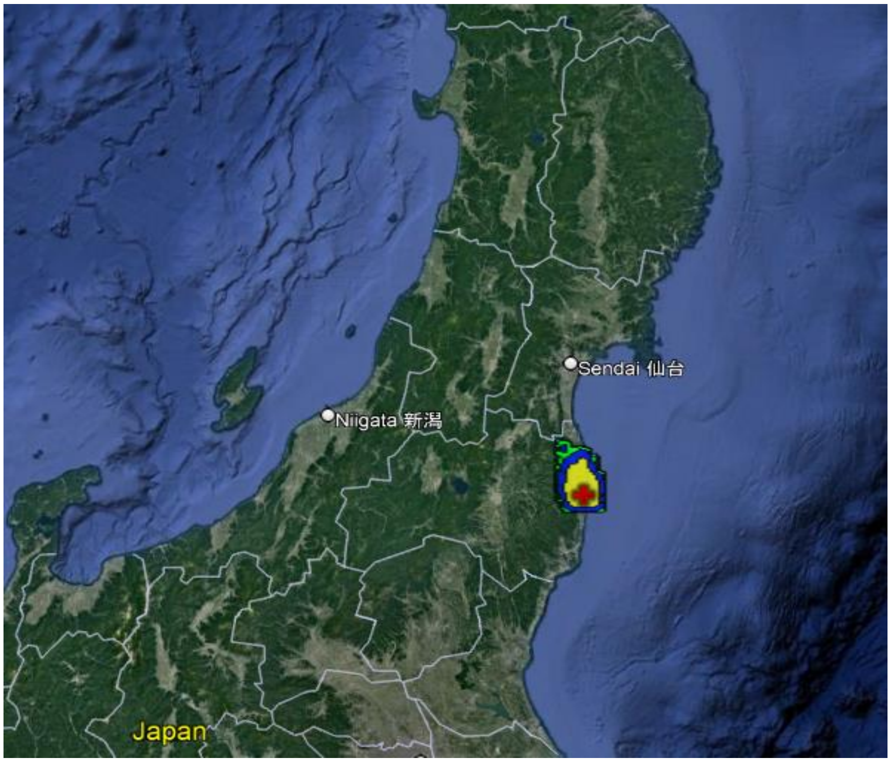

Figure 4-3. 2 hours into the wildfire

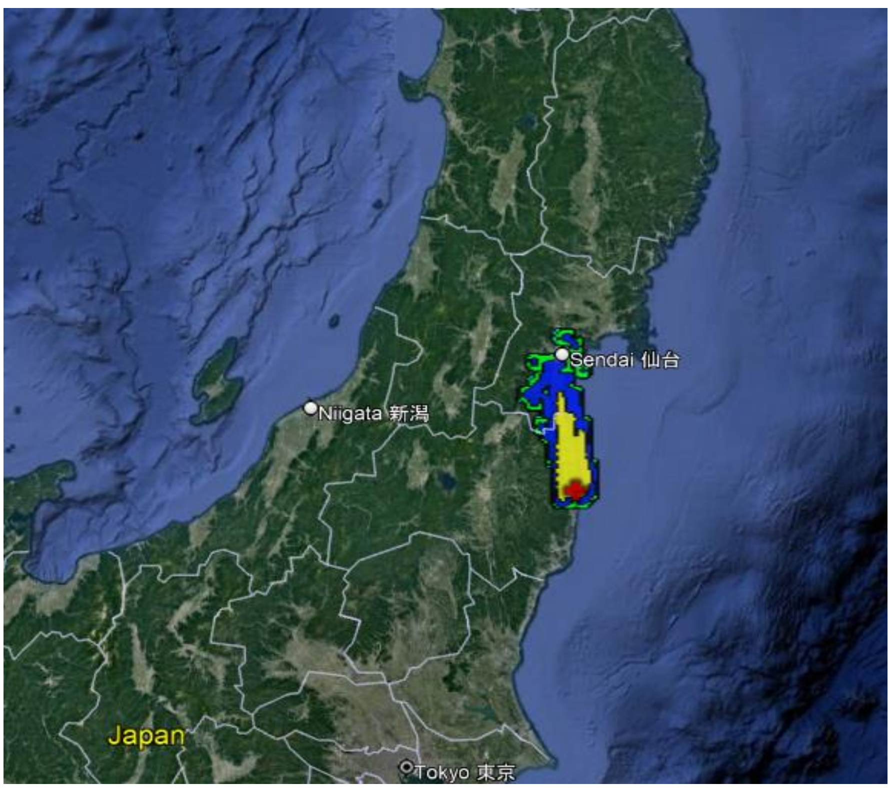

Figure 4-4. 6 hours into the wildfire

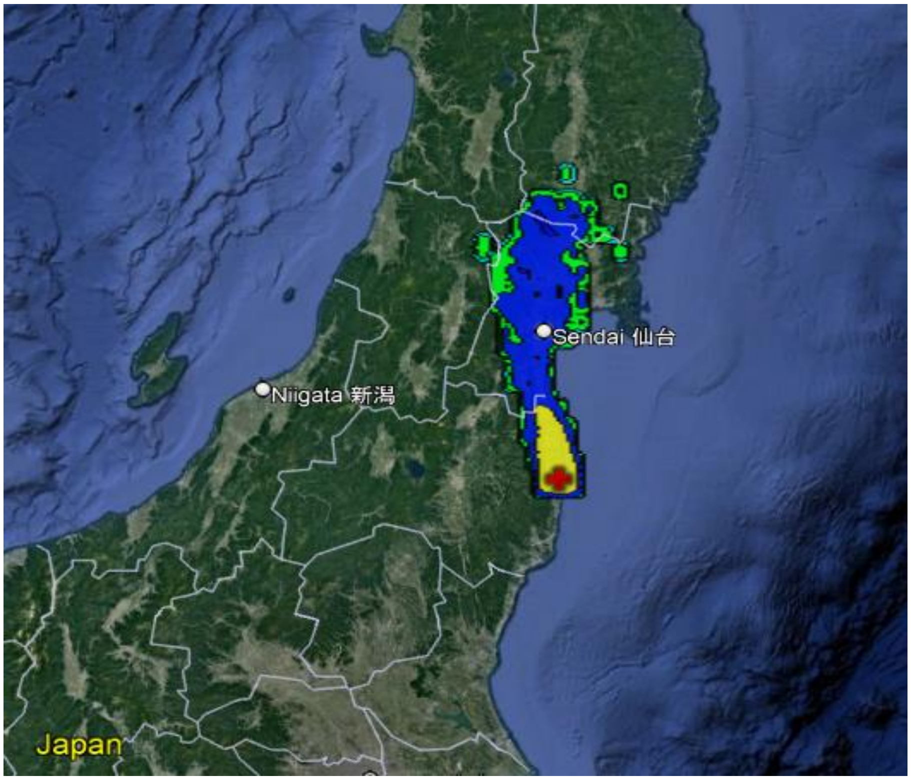

Figure 4-5. 10 hours into the wildfire

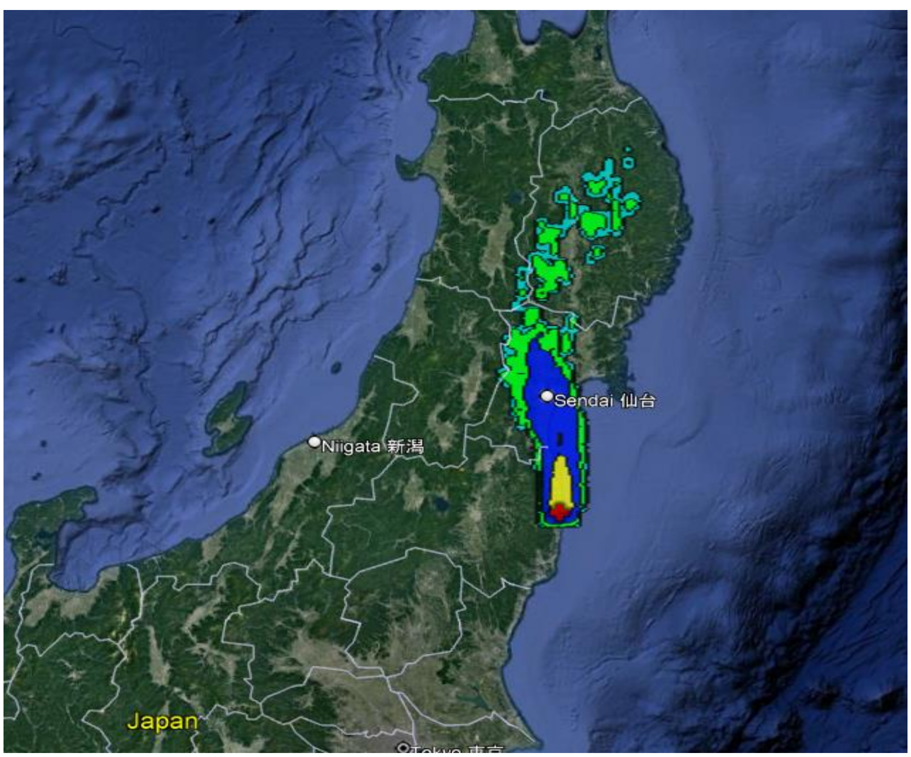

Figure 4-6. 14 hours into the wildfire

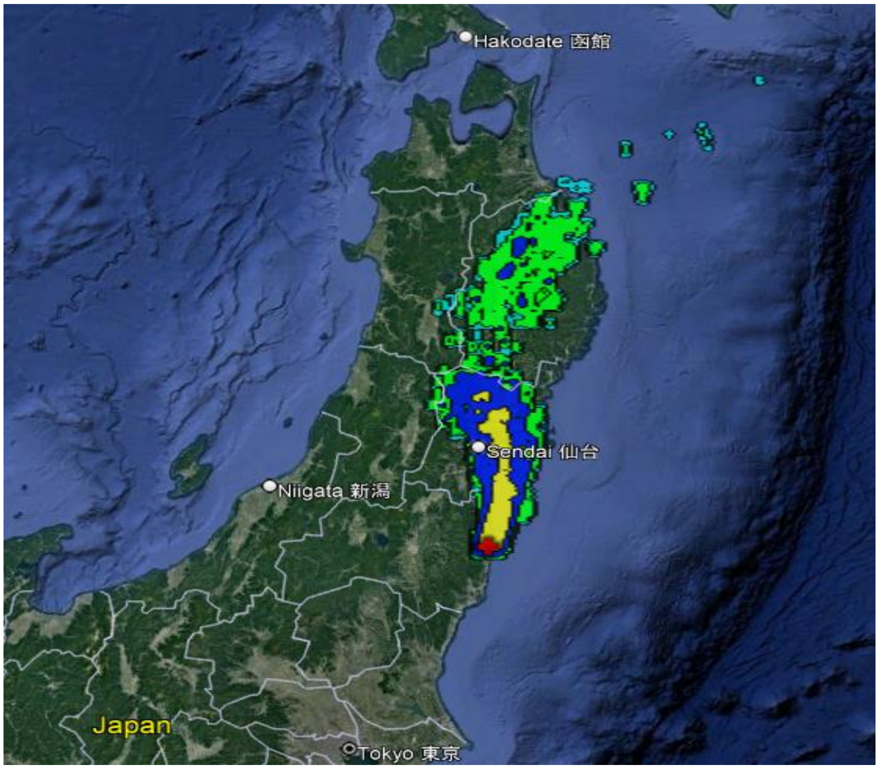

Figure 4-7. 18 hours into the wildfire

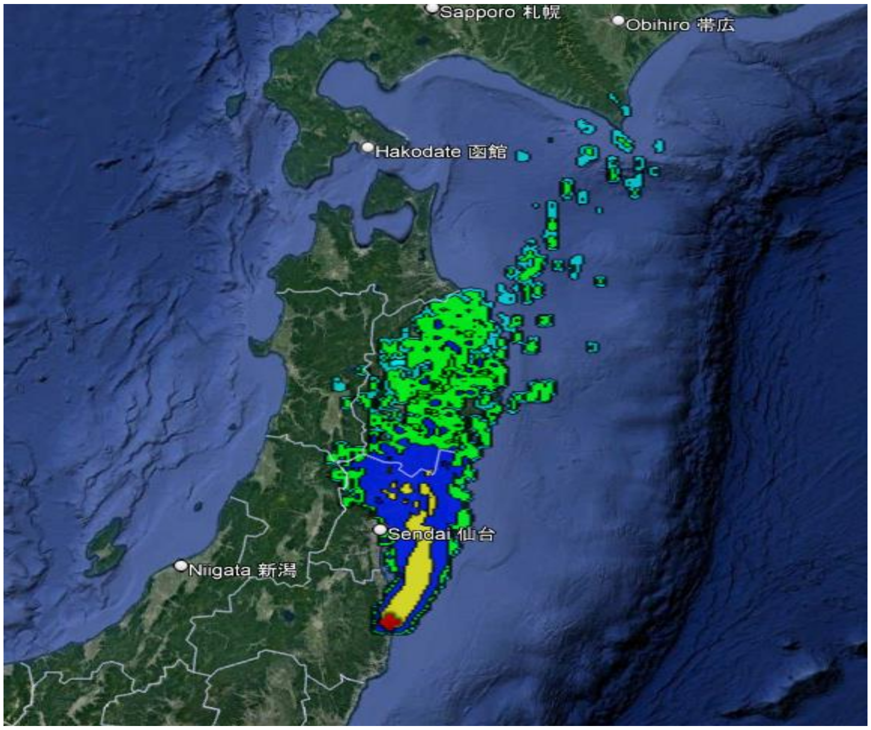

Figure 4-8. 22 hours into the wildfire

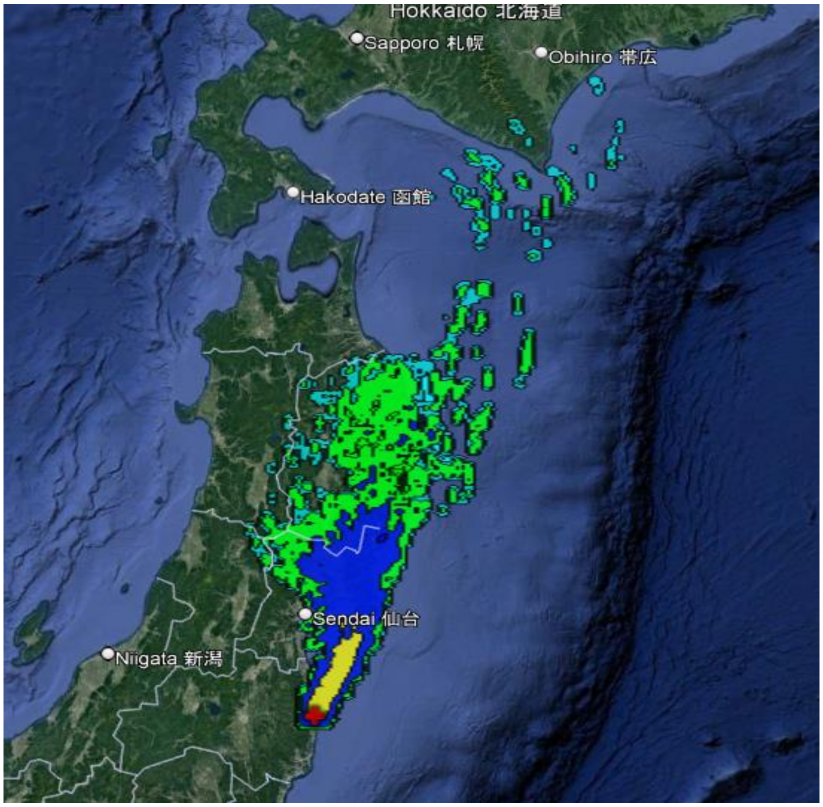

Figure 4-9. 24th hour, end of the wildfire

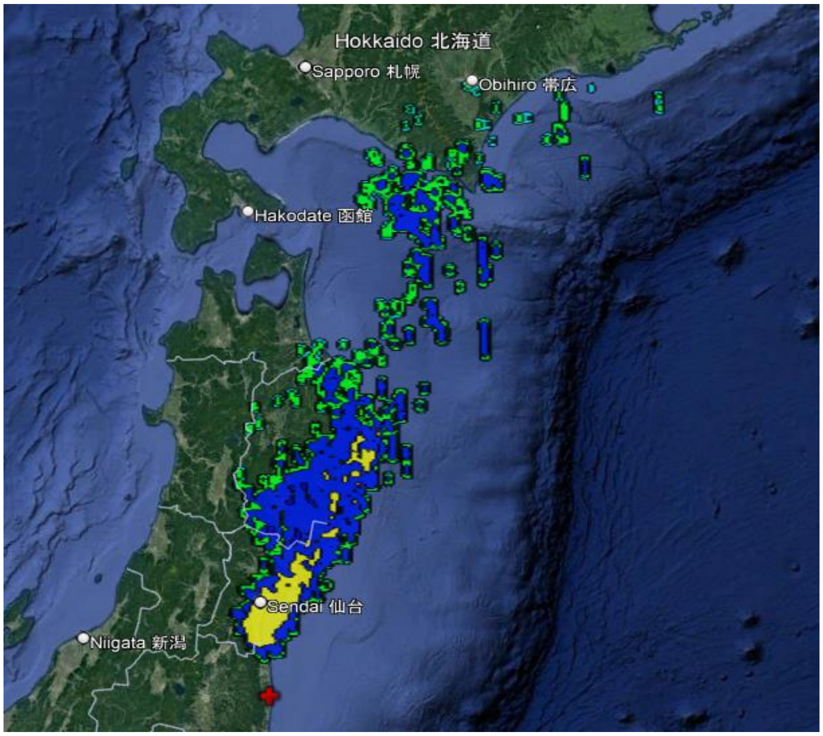

Figure 4-10. 28th hour, 4 hours after the wildfire ended

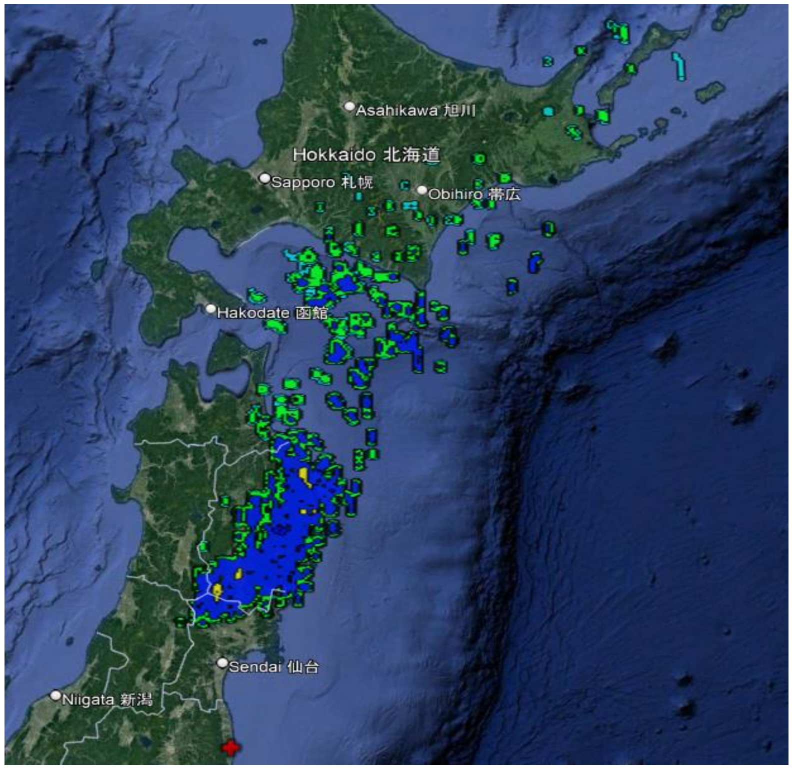

Figure 4-11. 32nd hour, 6 hours after the wildfire

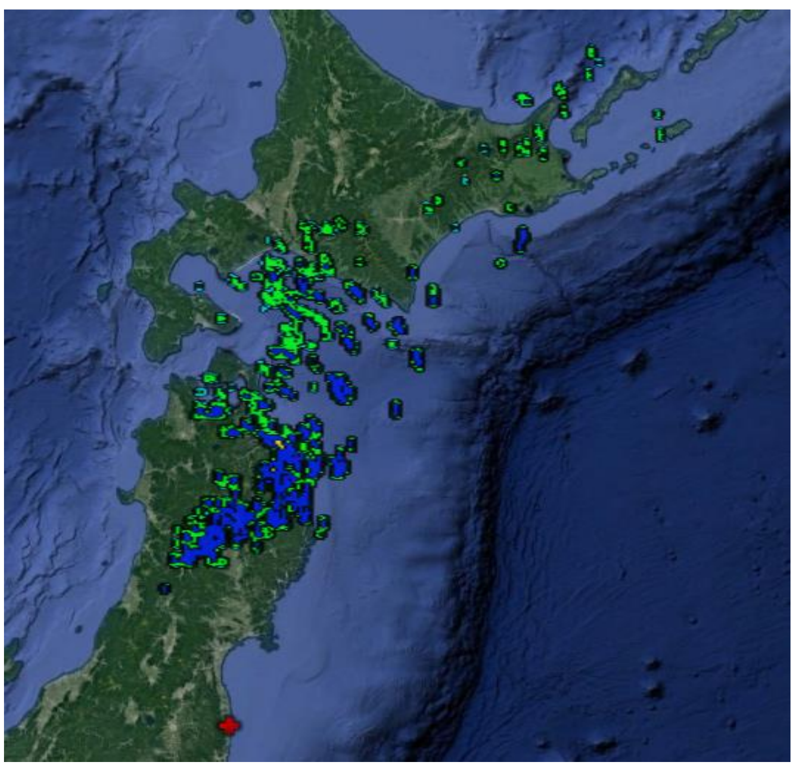

Figure 4-12. 36th hour, 10 hours after the wildfire

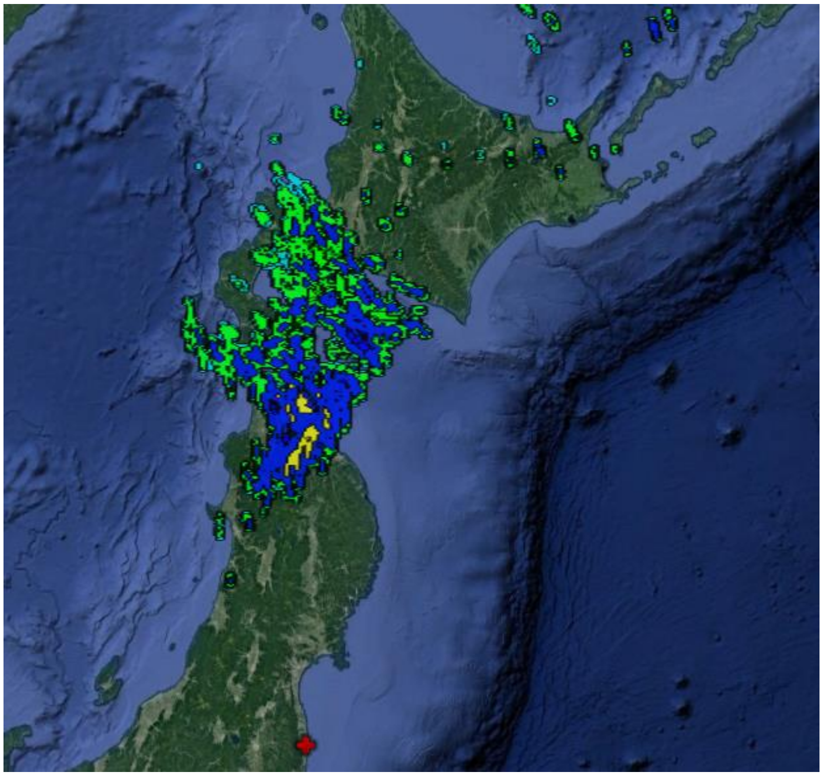

Figure 4-13. 42nd hour, 16 hours after the wildfire

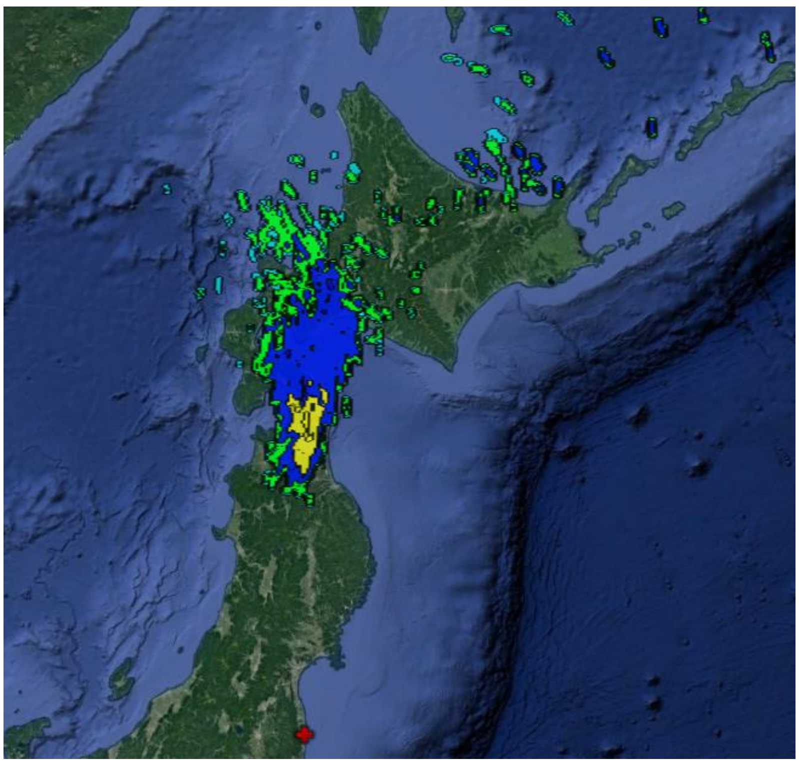

Figure 4-14. 44th hour, 18 hours after the wildfire

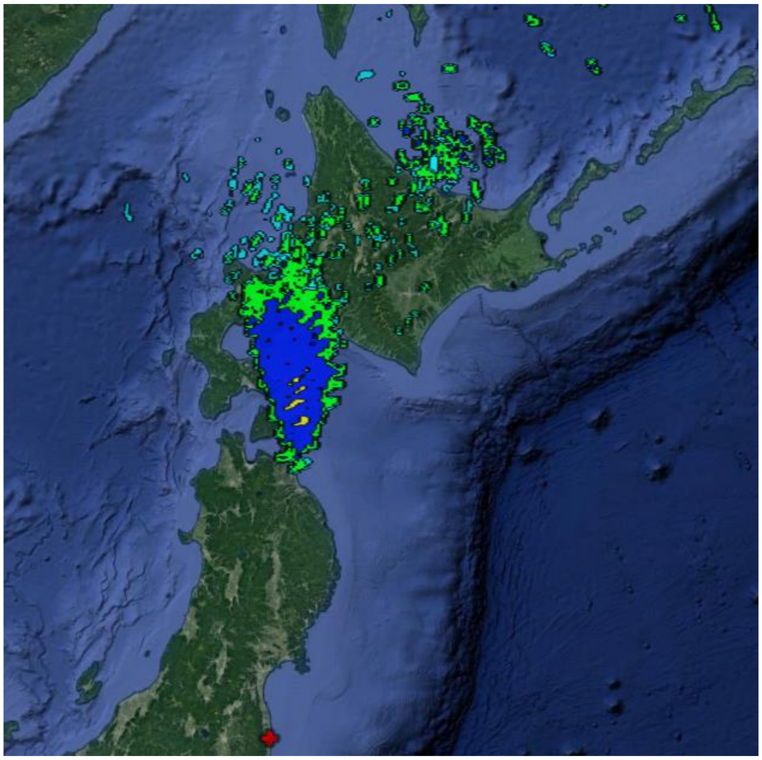

Figure 4-15. 46th hour, 22 hours after the wildfire

4.4.1. Inhalation Exposure Dose

Inhalation exposure appears to be the biggest contributor to the total dose calculations. To calculate the inhalation values, the effective dose rate was calculated by using the maximum air concentration value from the HYSPLIT results.

$$D_{inh}^{i} = \left[C_{air}^{i} \times InhR \times DCC_{inh}^{i}\right]_{outdoor} + \left[0.4\ (C_{air}^{i} \times InhR \times DCC_{inh}^{i})\right]_{indoor} \qquad (4.1)$$

In this model, which is used by taking the NRC as a reference, the total intake is found by using the measured air concentration, breathing rate, and time, and then the inhalation dose is found by multiplying the total intake by the inhalation dose coefficient. The inhalation dose coefficient of 4.6E-09 Sv/Bq was taken from ICRP 60[63], for the value of fast absorbent (F type), which is the recommended default absorption type of Cs-137 according to ICRP 72[64], used for adult individuals was used.

The general formula given in Equation *(3.25)* in the theoretical model section gives us the cumulative dose amount taken at the end of the elapsed time. Since the hourly maximum air concentration is known, without multiplying this formula with the time factor while making the calculations, we evaluated our results as dose rates (dose/hour). Afterward, the total effective dose taken at the end of 48 hours period was calculated using the elapsed time and hourly measured air concentrations by taking into account outdoor times and indoor times with a reduction factor of 0.4 as the Japanese government used for the calculations of accident by referring the IAEA.[30,31]

In Figure 4-16, there are inhalation dose rates showing the fire lasting 24 hours and the following 24 hours. The dose reached the highest level in the last hour of the fire. According to the assumptions made, the maximum dose rate with the lowest release amount is 8.5 μSv/hr, while the maximum dose rate with the highest release is 25.5 μSv/hr.

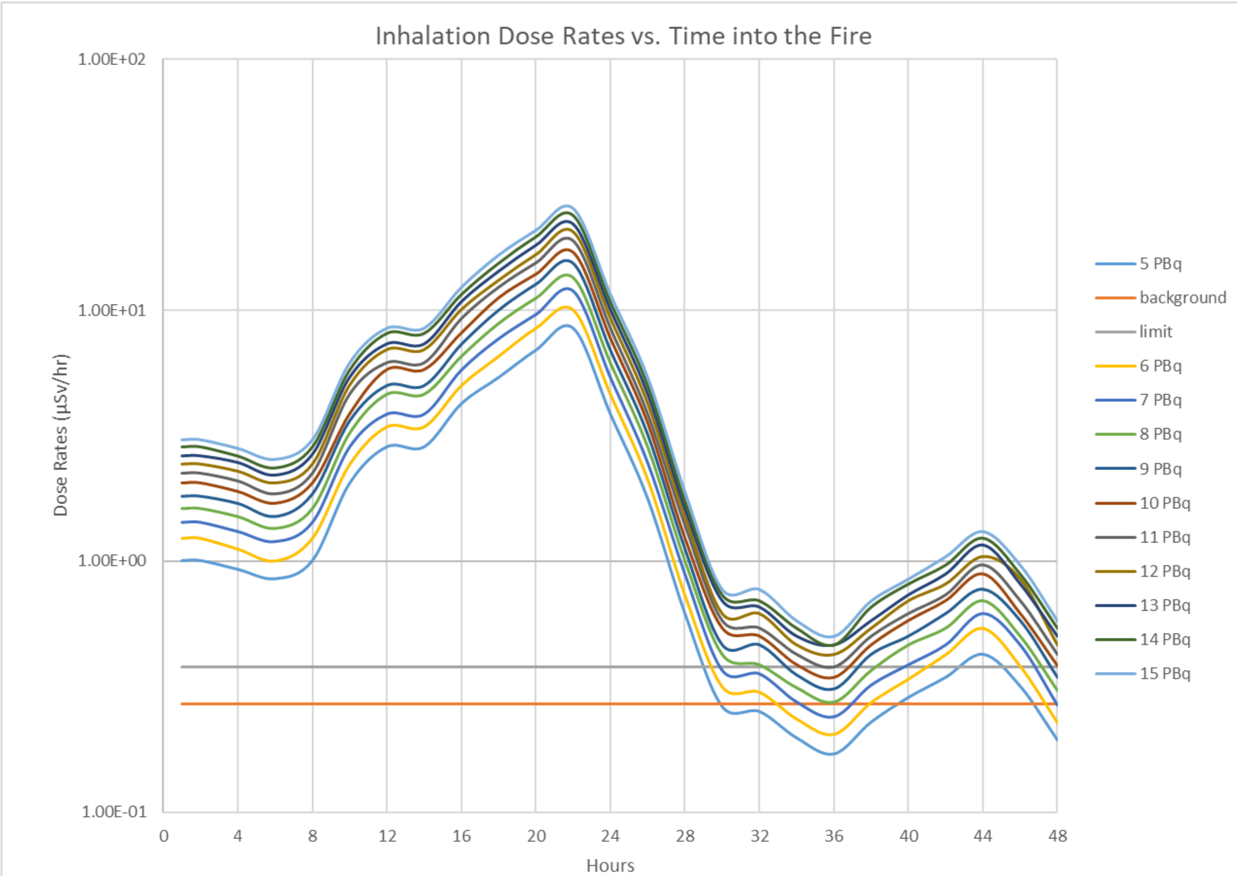

Figure 4-16. Inhalation dose rates

The observed peak in the graph after the fire was due to fluctuations in the weather. This peak can be explained by the fact that the air condenses at one point and gives high concentration values due to the wind.

4.4.2. Cloud-Shine Exposure Dose

In cloud-shine exposure, the effect of the plume will lose its effectiveness because of the deposition of some of the radionuclides on the way it passes, depending on the ground structure. However, the indoor and outdoor times of the recipient also allow for corrections in the dose calculation. In the calculation made in this study, it was assumed that the recipient, who was assumed to spend half of the day indoors and the other half outdoors, received half of the calculated dose and reduced dose for the indoor times. The model used to calculate the cloud-shine exposure dose is as follows.

$$D^i_{cld} = \left[C^i_{air} \times DCC^i_{cld}\right]_{outdoor} + \left[0.4\left(C^i_{air} \times DCC^i_{cld}\right)\right]_{indoor} \tag{4.2}$$

A similar path with inhalation in cloud-shine exposure is seen in Figure 4-17. However, the amount of radiation received in this way is much less compared to inhalation and remains well below the limit or background values even at the highest release amount.

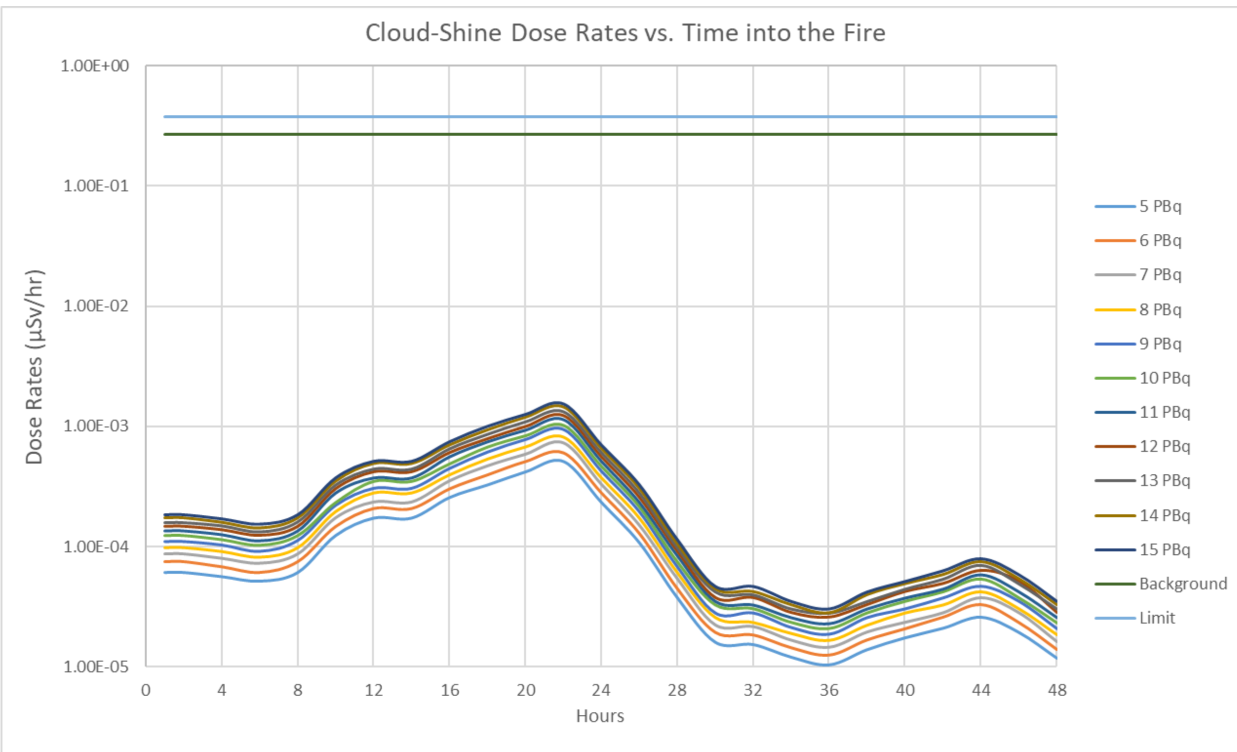

Figure 4-17. Cloud-shine dose rates

Although the effect is very low, the maximum contribution of cloud-shine exposure is 1.54e-3 µSv/hr.

4.4.3. Ground-Shine Exposure Dose

In ground-shine exposure, because of the deposition of radionuclides spread to the environment after the fire, the population living on or passing through the ground is exposed to this radiation externally. Where deposition is a collective term, the dose taken increases over time. Again, indoor, and outdoor times are considered in order to make corrections in the calculations. The formula used to calculate the ground-shine exposure dose is as follows.

$$D_{grd}^{i} = \left[CL_{ground}^{i} \times GCC_{grd}^{i}\right]_{outdoor} + \left[0.4\ (CL_{ground}^{i} \times GCC_{grd}^{i})\right]_{indoor} \tag{4.3}$$

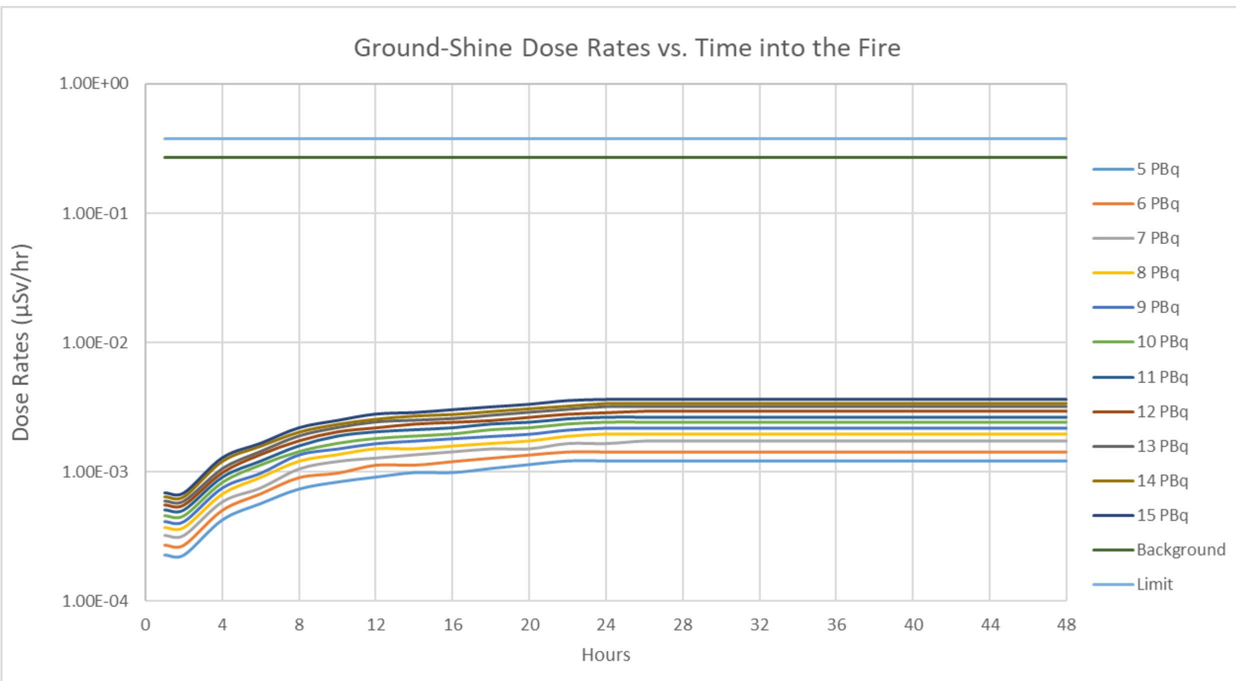

Figure 4-18. Ground-shine dose rates

For ground-shine exposure, dose rates are similar to cloud-shine and remain below the background and limit even at the highest release. However, the path in the graphic differs from cloud-shine and inhalation, as there is a deposition for ground shine. In this graph, we see the dose rate is increasing over time based on cumulative deposition on the ground. However, an important point for ground-shine is that this type of exposure continues after a fire. While inhalation and cloud-shine exposure approach zero with the subside of radioactive particles in the air, ground-shine exposure continues as it will take longer for the particles on the ground to penetrate the soil or be washed away by precipitation.

The situation for ground-shine exposure is the same as for cloud-shine, and we cannot say that it has any significant effect on the total dose. Even with the highest emission its maximum contribution is 3.63e-3 μSv/hr. The difference between them is that since cloud-shine originates from plume, its effect is gradually decreasing, and although its graph is comparable to the inhalation graph, the graph of ground-shine exposure is constantly increasing, but after the end of the fire, it increases with a lower slope and follows a linear line.

4.4.4. Ingestion Exposure Dose

Ingestion exposure is one of the biggest contributors to future health dose assessments because the contaminated soil and water continue to contaminate the food or drinking water for years. Restricting the intake of local food and drink immediately after the accident significantly reduced the radiation received in this way but did not eliminate entirely. It is known that the wild forest food consumption of the Japanese people is high. Therefore, it is possible to spread the resuspended radionuclides with a fire that may occur, and to mix and consume again from the air to drinking water, local food, and milk. However, considering that the same restrictions will be imposed in the event of such a fire, we can also assume that the risk of ingestion is not high compared to other exposure ways in this case.

4.4.5. Total and Cumulative Dose

The total dose rate is found by summing all the exposure paths for all the elements involved in the calculation. The hourly rate of the total dose received due to exposure of Cs-137 by inhalation, cloud-shine, and ground-shine is presented in the graphic below.

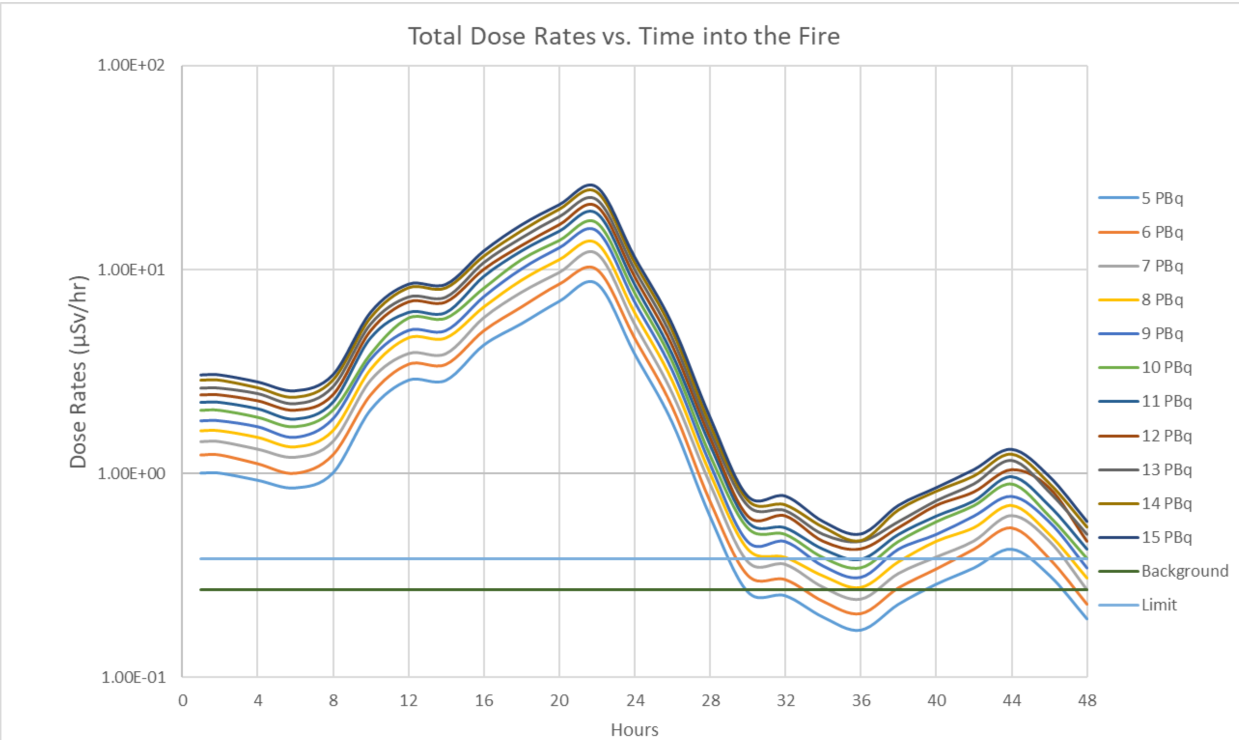

Figure 4-19. Total dose rates

According to the total dose rate graph, the maximum dose rate in the highest release is seen as 25.5 µSv. Here, we can say that inhalation is the only major effect because the dose rates of ground-shine and cloud-shine exposure thousands lower than inhalation exposure.

The cumulative dose is the sum of all exposures to which individuals are exposed over time. The cumulative dose calculated in the study is the sum of inhalation, cloud-shine, and ground-shine doses. Since inhalation is the biggest contributor here, even if other doses are below the limits, when considered cumulatively, the dose to which the surrounding public is exposed in case of such a fire is above the limits. As seen in the cumulative dose chart below, the dose taken after the fire has ended, although there are peak areas on the inhalation chart, shows a linear curve as its effect is very low.

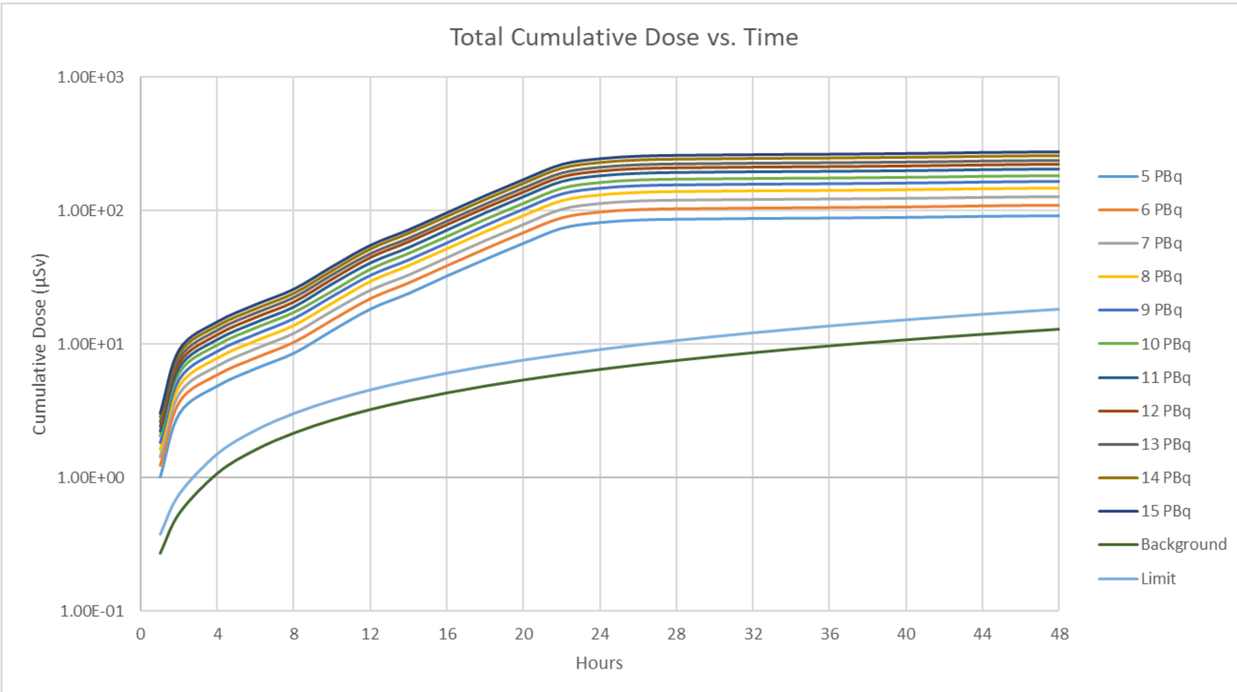

Figure 4-20. Cumulative dose received for 48 hours

At the total cumulative dose, a maximum of 277 μSv exposure is achieved with the highest emission at the end of 48 hours with the assumption of half indoor and half outdoor time, while 92.3 μSv exposure is achieved with the lowest emission. Cumulative dose shows the sum of the dose exposed during the whole wildfire, so according to our scenario, the maximum dose that an individual living in the region will receive during this fire is 277 μSv. If compared, this dose amount with the doses exposed in the medical applications explained before, this dose is equivalent to the followings for two-day time window,

– Three Chest X-rays.
– 1.5 times of one head CT scan.
– Roughly 19 dental X-rays.
– 21 times the normal background radiation.

- Roughly equivalent to 100 hours of air travel in two days.

None of these doses are fatal or serious. But the kinds of amounts we would try to avoid exposure in two days, and maybe even over a long period of time, when we look at each. Since the effects of low-dose radiation are not certain, it is not possible to give a definite conclusion about the possible effects on health in the short or long term.

5. DISCUSSION AND FUTURE WORK

In this study, a general framework about the health effects of fires that may occur in contaminated areas was created and the risk assessment and planning steps that should be done for effective response to such fires. A fire scenario for the Fukushima region was constructed as an example and demonstrated the potential effected areas from the fire by modeling atmospheric dispersion. As a result of this distribution, calculations of how much dose a person living in the environment would be exposed to were computed. According to those calculations, the highest dose found was 277 μSv, and this dose is not a dose which effects on health are known with certainty, as shown in Section 3.4.1. To see the effects of radiation on human health, it must be exposed to much higher doses than 277 μSv.

Moreover, the fires that broke out around Chernobyl for years are still worry about the surrounding population and nearby nations. The study also revealed that these fires are not a major source of concern, but nevertheless, these concerns can be alleviated with significant emergency planning and information. The fact that the authorities of the regions around which contain contaminated areas have this planning in advance and informing the people living in that region about this planning will eliminate their concerns and provide an effective response against both fire and radiological contamination.

As seen in the study, inhalation is the exposure pathway that contributes the highest to the dose taken. In this case, even a simple shelter-in-place measure will greatly protect the public from this dose. In addition, this study gave similar results with Kashparov's study on forest fires around Chernobyl in terms of dose rates when the parameters are taken into account.[65] However, the spread of the fire we modeled here over a much larger area compared to the fire test conducted in Chernobyl showed that a larger area would be affected in a real fire situation. In the event of such a fire, there is a risk that previously unaffected areas may be contaminated with the transported radioactive ash. Therefore, carrying out a comprehensive risk assessment and emergency planning study in these areas is necessary and valuable both for the health of the people living in contaminated areas and for the non-contamination of clean areas.

This study shows only the distribution of the Cs-137 particle and the radiation received by inhalation, cloud-shine exposure, and ground-shine exposure pathways. The dispersion of ash and other particles that may be emitted by fire or their effects on human health, and the radiation exposure over time through ingestion have not been calculated. Therefore, the results of these parameters are not available in this study and the study is open to improvement in these aspects. In addition, although our study focused on radioactively contaminated areas, it created a framework that could be used in areas contaminated by other pollutants.

6. CONCLUSION

This thesis characterized the transportation, dispersion, and deposition of Cs-137 that will resuspend in the event of a fire around Fukushima. Using modeling, the study proved that the concentration of Cs-137 in the air exceeds the background and limit values. From the model the opportunity to predict the environmental consequences is available. The results of the analysis showed that the total exposed dose was not at a level that would pose a hazard, but the effect of the inhalation additive on the total dose was large in the case of resuspension. With the literature review, the lack of an additional probabilistic risk assessment study for contaminated areas was obvious and presented a general framework for a risk-informed emergency planning. Thus, this study explains that in wildfires in contaminated areas, a radiological hazard is not encountered if an effective emergency response plan is in place. Otherwise, it is possible that not knowing how to manage the situation and delay in taking simple measures may have minor radiological consequences.

7. REFERENCES

[1] 2021, "IAEA Annual Report for 2020" [Online]. Available: https://www.iaea.org/opic/annual-report-2020. [Accessed: 21-Jun-2022].

[2] Kaplan, S., and Garrick, B. J., 1981, "On The Quantitative Definition of Risk," Risk Analysis, **1**(1), pp. 11–27.

[3] "WASH-1400 – The Reactor Safety Study – The Introduction of Risk Assessment to the Regulation of Nucl," NRC Web [Online]. Available: https://www.nrc.gov/reading-rm/doc-collections/nuregs/knowledge/km0010/index.html. [Accessed: 31-Aug-2021].

[4] Breeding, R. J., Helton, J. C., Murfin, W. B., Smith, L. N., Johnson, J. D., Jow, H.-N., and Shiver, A. W., 1992, "The NUREG-1150 Probabilistic Risk Assessment for the Surry Nuclear Power Station," Nuclear Engineering and Design, **135**(1), pp. 29–59.

[5] "§ 50.47 Emergency Plans.," NRC Web [Online]. Available: https://www.nrc.gov/reading-rm/doc-collections/cfr/part050/part050-0047.html. [Accessed: 21-Jun-2022].

[6] De Meutter, P., Gueibe, C., Tomas, J., Outer, P. den, Apituley, A., Bruggeman, M., Camps, J., Delcloo, A., Knetsch, G.-J., Roobol, L., and Verheyen, L., 2021, "The Assessment of the April 2020 Chernobyl Wildfires and Their Impact on Cs-137 Levels in Belgium and The Netherlands," Journal of Environmental Radioactivity, **237**, p. 106688.

[7] "International Nuclear and Radiological Event Scale (INES) | IAEA" [Online]. Available: https://www.iaea.org/resources/databases/international-nuclear-and-radiological-event-scale. [Accessed: 11-Jun-2021].

[8] 2011, "Fukushima Nuclear Accident Update Log" [Online]. Available: https://www.iaea.org/newscenter/news/fukushima-nuclear-accident-update-log-15. [Accessed: 21-Jun-2022].

[9] INTERNATIONAL ATOMIC ENERGY AGENCY and VIENNA, 1996, *ONE DECADE AFTER CHERNOBYL Summing up the Consequences of the Accident*.

[10] United Nations and United Nations, 2011, *Sources and Effects of Ionizing Radiation, UNSCEAR 2008 Report*.

[11] Dreicer et al., 1996, "Consequences of the Chernobyl Accident for the Natural and Human Environments."

[12] Evangeliou, N., Balkanski, Y., Cozic, A., Hao, W. M., Mouillot, F., Thonicke, K., Paugam, R., Zibtsev, S., Mousseau, T. A., Wang, R., Poulter, B., Petkov, A., Yue, C., Cadule, P., Koffi, B., Kaiser, J. W., and Møller, A. P., 2015, "Fire Evolution in the Radioactive Forests of Ukraine and Belarus: Future Risks for the Population and the Environment," Ecological Monographs, **85**(1), pp. 49–72.

[13] United Nations, ed., 2000, *Sources and Effects of Ionizing Radiation: United Nations Scientific Committee on the Effects of Atomic Radiation: UNSCEAR 2000 Report to the General Assembly, with Scientific Annexes*, United Nations, New York.

[14] "TEPCO : Press Release | Payment of Temporary Compensation for Damages Caused by Evacuation" [Online]. Available: https://www.tepco.co.jp/en/press/corp-com/release/11041501-e.html. [Accessed: 21-Jun-2022].

[15] 2014, *Sources, Effects and Risks of Ionizing Radiation, Unscear 2013 Report Levels and Effects of Radiation Exposure Due to the Nuclear Accident After the 2011 Great East-Japan Earthquake ...*, United Nations Pubns.

[16] "The Fukushima Daiichi Accident" [Online]. Available: https://www.irsn.fr/EN/publications/thematic-safety/fukushima/Pages/overview.aspx. [Accessed: 21-Jun-2022].

[17] "Fukushima, One Year Later - Initial Analyses of the Accident and Its Consequences," p. 188.

[18] 2015, *The Fukushima Daiichi Accident Report by the Director General ; Technical Volume 1/5, Description and Context of the Accident ; Technical Volume 2/5, Safety Assessment ; Technical Volume 3/5, Emergency Preparedness and Response ; Technical Volume 4/5, Radiological Consequences ; Technical Volume 5/5, Post-Accident Recovery ; Annexes*, IAEA, Vienna.

[19] Internationale Atomenergie-Organisation, ed., 2015, *The Fukushima Daiichi Accident V1/5*, International Atomic Energy Agency, Vienna, Austria.

[20] Garrick, B. J., 2008, *Quantifying and Controlling Catastrophic Risks*, Academic Press.

[21] "EFFIS - Annual Fire Reports" [Online]. Available: https://effis.jrc.ec.europa.eu/reports-and-publications/annual-fire-reports. [Accessed: 22-Jun-2022].

[22] "Forestry Agency / How Many Wildfires Are There in Japan? : Forestry Agency" [Online]. Available: https://www.rinya.maff.go.jp/j/hogo/yamakaji/con_1.htm. [Accessed: 22-Jun-2022].

[23] "GLOBAL FOREST FIRE ASSESSMENT 1990-2000 - FRA WP 55" [Online]. Available: https://www.fao.org/3/ad653e/ad653e56.htm#P6731_454901. [Accessed: 22-Jun-2022].

[24] Vizzuality, "Japan Deforestation Rates & Statistics | GFW" [Online]. Available: https://www.globalforestwatch.org/dashboards/country/JPN?category=fires. [Accessed: 22-Jun-2022].

[25] "National Fire News | National Interagency Fire Center" [Online]. Available: https://www.nifc.gov/fire-information/nfn. [Accessed: 14-Jun-2022].

[26] "Wildfires and Acres | National Interagency Fire Center" [Online]. Available: https://www.nifc.gov/fire-information/statistics/wildfires. [Accessed: 14-Jun-2022].

[27] "Wildfires and Acres | National Interagency Fire Center" [Online]. Available: https://www.nifc.gov/fire-information/statistics/wildfires. [Accessed: 22-Jun-2022].

[28] Bozoki, G. E., Fitzpatrick, R. G., Bohn, M. P., Sabek, M. G., Ravindra, M. K., and Johnson, J. J., 1994, *Review of the Diablo Canyon Probabilistic Risk Assessment*, NUREG/CR--5726, BNL-NUREG--52288, 10181672.

[29] "NRC: 10 CFR Part 50—Domestic Licensing of Production and Utilization Facilities" [Online]. Available: https://www.nrc.gov/reading-rm/doc-collections/cfr/part050/. [Accessed: 04-Sep-2020].

[30] 2000, *Generic Procedures for Assessment and Response During a Radiological Emergency*, INTERNATIONAL ATOMIC ENERGY AGENCY, Vienna.

[31] “PLANNING FOR OFF-SITE RESPONSE TO RADIATION ACCIDENTS IN NUCLEAR FACILITIES,” p. 125.

[32] Prestemon, J. P., Hawbaker, T. J., Bowden, M., Carpenter, J., Brooks, M. T., Abt, K. L., Sutphen, R., and Scranton, S., 2013, “Wildfire Ignitions: A Review of the Science and Recommendations for Empirical Modeling,” Gen. Tech. Rep. SRS-GTR-171. Asheville, NC: USDA-Forest Service, Southern Research Station. 20 p., **171**, pp. 1–20.

[33] “Wildfires and Acres | National Interagency Fire Center” [Online]. Available: https://www.nifc.gov/fire-information/statistics/wildfires. [Accessed: 08-Jul-2022].

[34] Kashparov, V. A., Lundin, S. M., Kadygrib, A. M., Protsak, V. P., Levtchuk, S. E., Yoschenko, V. I., Kashpur, V. A., and Talerko, N. M., 2000, “Forest Fires in the Territory Contaminated as a Result of the Chernobyl Accident: Radioactive Aerosol Resuspension and Exposure of Fire-Fighters,” p. 18.

[35] Kashparov, V. A., Lundin, S. M., Zvarych, S. I., Yoshchenko, V. I., Levchuk, S. E., Khomutinin, Y. V., Maloshtan, I. M., and Protsak, V. P., 2003, “Territory Contamination with the Radionuclides Representing the Fuel Component of Chernobyl Fallout,” Science of The Total Environment, **317**(1–3), pp. 105–119.

[36] Evangeliou, N., Zibtsev, S., Myroniuk, V., Zhurba, M., Hamburger, T., Stohl, A., Balkanski, Y., Paugam, R., Mousseau, T. A., Møller, A. P., and Kireev, S. I., 2016, “Resuspension and Atmospheric Transport of Radionuclides Due to Wildfires near the Chernobyl Nuclear Power Plant in 2015: An Impact Assessment,” Sci Rep, **6**(1), p. 26062.

[37] CNN, R. P., “Chernobyl Radiation Levels Spike as Forest Fires Rage,” CNN [Online]. Available: https://www.cnn.com/2020/04/06/europe/chernobyl-fire-radiation-scli-intl-scn/index.html. [Accessed: 20-Jun-2022].

[38] Roach, S., 2022, “Chernobyl Forest Fires Raise Radiation Fears,” Protocol [Online]. Available: https://www.protocol.com/bulletins/forest-fire-chernobyl-radiation. [Accessed: 20-Jun-2022].

[39] Milman, O., 2022, “Forest Fires Erupt around Chernobyl Nuclear Plant in Ukraine,” The Guardian.

[40] “ESTIMATION OF RADIOACTIVE SOURCE TERM DYNAMICS FOR ATMOSPHERIC TRANSPORT DURING WILDFIRES IN CHERNOBYL ZONE IN SPRING 2020.”

[41] “Fires in Ukraine in the Exclusion Zone around the Chernobyl Power Plant: Latest Measurement Results and Assessment of Environmental and Health Consequences,” p. 10.

[42] Talerko, M., Kovalets, I., Lev, T., Igarashi, Y., and Romanenko, O., 2021, “Simulation Study of Radionuclide Atmospheric Transport after Wildland Fires in the Chernobyl Exclusion Zone in April 2020,” Atmospheric Pollution Research, **12**(3), pp. 193–204.

[43] Saito, K., Tanihata, I., Fujiwara, M., Saito, T., Shimoura, S., Otsuka, T., Onda, Y., Hoshi, M., Ikeuchi, Y., Takahashi, F., Kinouchi, N., Saegusa, J., Seki, A., Takemiya, H., and Shibata, T., 2015, “Detailed Deposition Density Maps Constructed by Large-Scale Soil Sampling for

Gamma-Ray Emitting Radioactive Nuclides from the Fukushima Dai-Ichi Nuclear Power Plant Accident," Journal of Environmental Radioactivity, **139**, pp. 308–319.

[44] International Atomic Energy Agency, 2020, *Environmental Transfer of Radionuclides in Japan Following the Accident at the Fukushima Daiichi Nuclear Power Plant: Report of Working Group 4 : Transfer Processes and Data for Radiological Impact Assessment Subgroup 2 on Fukushima Data : IAEA Programme on Modelling and Data for Radiological Impact Assessments (MODARIA II).*

[45] Kato, H., and Onda, Y., 2018, "Determining the Initial Fukushima Reactor Accident-Derived Cesium-137 Fallout in Forested Areas of Municipalities in Fukushima Prefecture," Journal of Forest Research, **23**(2), pp. 73–84.

[46] Draxler, R. R., and Hess, G. D., "NOAA Technical Memorandum ERL ARL-224," p. 31.

[47] Stein, A. F., Draxler, R. R., Rolph, G. D., Stunder, B. J. B., Cohen, M. D., and Ngan, F., 2015, "NOAA's HYSPLIT Atmospheric Transport and Dispersion Modeling System," Bulletin of the American Meteorological Society, **96**(12), pp. 2059–2077.

[48] Draxler, R., Stunder, B., Rolph, G., Stein, A., and Taylor, A., "HYSPLIT User's Guide," p. 249.

[49] Zoellick, C. L., "Source Term Estimation of Atmospheric Pollutants Using an Ensemble of HYSPLIT Concentration Simulations," p. 111.

[50] US EPA, O., 2015, "Radiation Sources and Doses" [Online]. Available: https://www.epa.gov/radiation/radiation-sources-and-doses. [Accessed: 30-May-2022].

[51] "Health Effects of Radiation: 5 Themes - (vi) Comparison of Exposure Doses in Daily Life" [Online]. Available: https://www.env.go.jp/en/chemi/rhm/portal/digest/travel/detail_006.html. [Accessed: 20-Jun-2022].

[52] Lamarsh, J. R., and Anthony J., B., *Introduction to Nuclear Engineering*, Prentice Hall PTR.

[53] "Doses in Our Daily Lives," NRC Web [Online]. Available: https://www.nrc.gov/about-nrc/radiation/around-us/doses-daily-lives.html. [Accessed: 27-Jun-2022].

[54] 1975, *NUREG-75/014, "Reactor Safety Study, An Assessment of Accident Risks in U.S. Commercial Nuclear Power Plants, Appendix VI."*

[55] "Airborne Particle Resuspension and Inhalation Radiological Dose Estimation Following Volcanic Events.," p. 15.

[56] Satoh, K., Song Weiguo, and Yang, K. T., 2004, "A Study of Forest Fire Danger Prediction System in Japan," *Proceedings. 15th International Workshop on Database and Expert Systems Applications, 2004.*, IEEE, Zaragoza, Spain, pp. 598–602.

[57] Internationale Atomenergie-Organisation, ed., 2015, *The Fukushima Daiichi Accident V 4/5*, International Atomic Energy Agency, Vienna, Austria.

[58] Stohl, A., Seibert, P., Wotawa, G., Arnold, D., Burkhart, J. F., Eckhardt, S., Tapia, C., Vargas, A., and Yasunari, T. J., 2012, "Xenon-133 and Caesium-137 Releases into the Atmosphere from the Fukushima Dai-Ichi Nuclear Power Plant: Determination of the Source Term, Atmospheric Dispersion, and Deposition," Atmos. Chem. Phys., **12**(5), pp. 2313–2343.

[59] "Evangeliou et al. - 2014 - Global and Local Cancer Risks after the Fukushima .Pdf."
[60] "Katata et al. - 2012 - Atmospheric Discharge and Dispersion of Radionucli.Pdf."
[61] Hashimoto, S., Ugawa, S., Nanko, K., and Shichi, K., 2012, "The Total Amounts of Radioactively Contaminated Materials in Forests in Fukushima, Japan," Sci Rep, **2**(1), p. 416.
[62] Baes, F., "Hps.Org," Health Physics Society [Online]. Available: http://hps.org/. [Accessed: 21-Jun-2022].
[63] "P 119 JAICRP 41(s) Compendium of Dose Coefficients Based on ICRP Publication 60.Pdf."
[64] Smith, H., "Published on Behalf of the Lnternational Commission on Radiological Protection," p. 108.
[65] Yoschenko, V. I., Kashparov, V. A., Protsak, V. P., Lundin, S. M., Levchuk, S. E., Kadygrib, A. M., Zvarich, S. I., Khomutinin, Yu. V., Maloshtan, I. M., Lanshin, V. P., Kovtun, M. V., and Tschiersch, J., 2006, "Resuspension and Redistribution of Radionuclides during Grassland and Forest Fires in the Chernobyl Exclusion Zone: Part I. Fire Experiments," Journal of Environmental Radioactivity, **86**(2), pp. 143–163.